Iron associated lipid peroxidation in Alzheimer's disease is increased in lipid rafts with decreased ferroptosis suppressors, tested by chelation in mice

Max A. Thorwald[1*], Jose A. Godoy-Lugo[1], Gilberto Garcia[1], Justine Silva[2], Minhoo Kim[1], Amy Christensen[1], Wendy J. Mack[3], Elizabeth Head[2], Peggy A. O'Day[4], Bérénice A. Benayoun[1], Todd E. Morgan[1], Christian J. Pike[1], Ryo Higuchi-Sanabria[1], Henry Jay Forman[1,5], Caleb E. Finch[1,6]

[1]Leonard Davis School of Gerontology, University of Southern California, Los Angeles, CA.
[2]Department of Pathology and Laboratory Medicine, University of California, Irvine, CA.
[3]Department of Pediatrics, Keck School of Medicine of the University of Southern California, Los Angeles, CA.
[4]Life and Environmental Sciences Department, University of California, Merced, CA.
[5]School of Natural Sciences, University of California Merced, Merced, CA.
[6]Dornsife College, University of Southern California, Los Angeles, CA.

ABSTRACT: Iron-mediated cell death (ferroptosis) is a proposed mechanism of Alzheimer's disease (AD) pathology. While iron is essential for basic biological functions, its reactivity generates oxidants which contribute to cell damage and death. To further resolve mechanisms of iron-mediated toxicity in AD, we analyzed postmortem human brain and ApoEFAD mice. AD brains had decreased antioxidant enzymes, including those mediated by glutathione (GSH). Subcellular analyses of AD brains showed greater oxidative damage and lower antioxidant enzymes in lipid rafts, the site of amyloid processing, than in the non-raft membrane fraction. ApoE4 carriers had lower lipid raft yield with greater membrane oxidation. The hypothesized role of iron to AD pathology was tested in ApoEFAD mice by iron chelation with deferoxamine, which decreased fibrillar amyloid and lipid peroxidation, together with increased GSH-mediated antioxidants. These novel molecular pathways in iron mediated damage during AD.

Keywords: GPx4, GCLM, FSP1, HNE, Ferritin, Deferoxamine, EFAD, amyloid

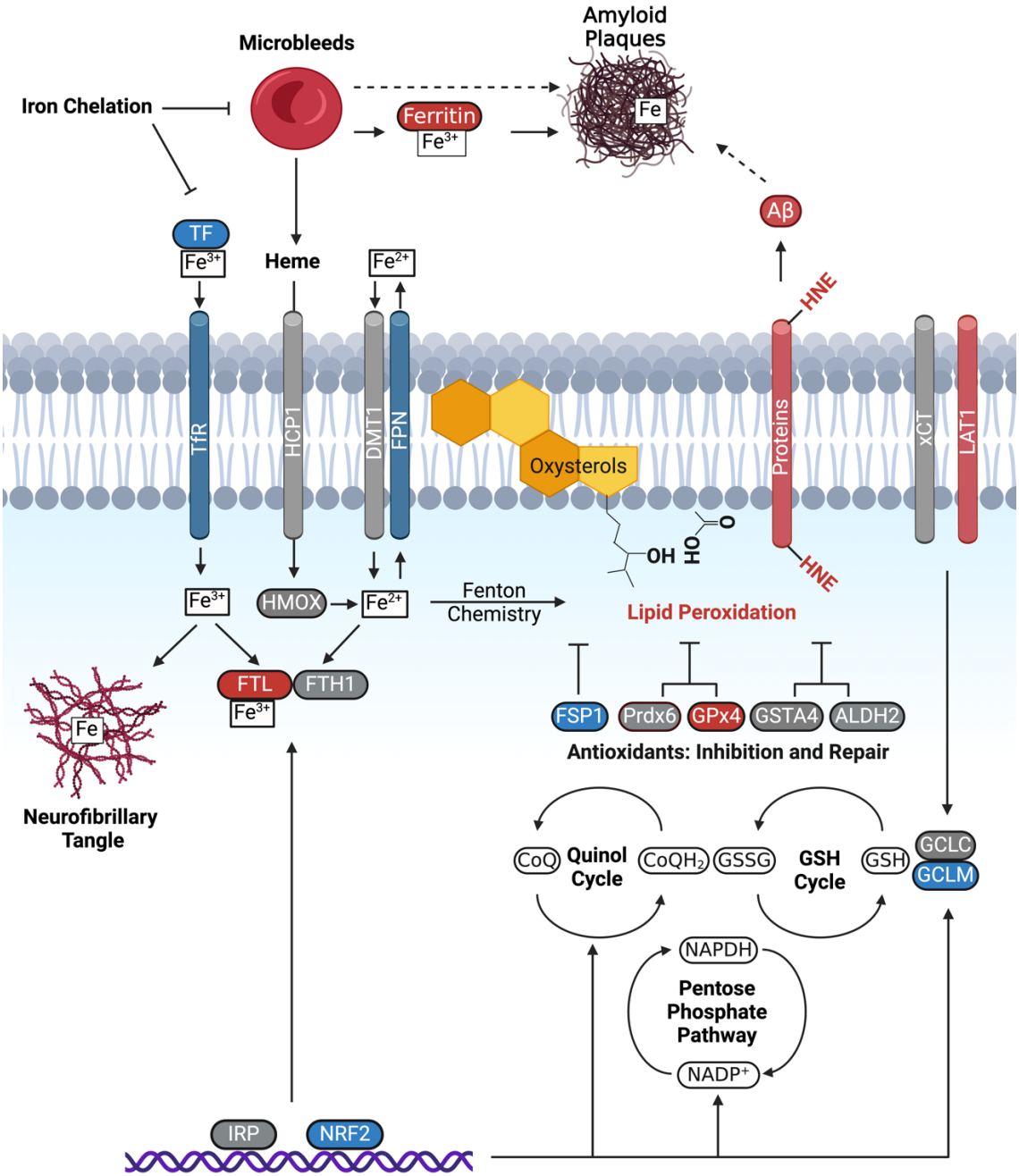

Graphical Abstract: Hypothesis: AD brain lipid peroxidation is driven by increased brain iron and decreased antioxidant defenses. Schema shows proteins that mediate iron metabolism in relation to lipid peroxidation (HNE) and antioxidant defenses in prefrontal cortex. AD-associated increase (red), decrease (blue), or no change (grey), relative to cognitively normal elderly controls. Aβ; amyloid beta, ALDH2; alcohol dehydrogenase, APP; amyloid precursor protein, DMT1; divalent metal transporter 1; FPN, ferroportin; FSP1, ferroptosis suppressor protein 1, which requires the quinol cycle to attenuate lipid peroxidation; FTH1, ferritin heavy chain; FTL; ferritin light chain; GCLC, glutathione cysteine ligase catalytic subunit; GCLM, glutathione cysteine ligase modulator; GPx4, glutathione peroxidase 4; GSH, glutathione; GSSG, glutathione disulfide; GSTA4, glutathione S-transferase A4; HMOX; heme oxygenase; IRP, iron regulatory protein; LAT1, large neutral amino acid transporter 1; LOOH, Lipid hydroperoxides; Nrf2, Nuclear factor erythroid 2-related factor 2; Prdx6, peroxiredoxin 6; TF, transferrin, TfR; Transferrin receptor; xCT, cysteine-glutamate antiporter.

63 **INTRODUCTION:**

64 Postmortem AD neuropathology is traditionally measured using two protein-aggregation
65 related biomarkers: accumulation of amyloid plaques and neurofibrillary tangles (NFT). However, less
66 than 35% of terminal cognitive decline was attributable to these neuropathological markers and was
67 weakly correlated with cognitive status in two large longitudinal studies[1,2]. We suggest new
68 mechanisms for the role of iron in AD neuropathology mediated by glutathione (GSH) and iron export.

69 Ferroptosis was first designated for cell death *in vitro* from inhibition of cystine glutamate
70 importer (xCT) essential for GSH biosynthesis by quinazoline erastin[3]. GSH is used body wide as an
71 essential substrate for the enzymatic reduction or removal of peroxides, HNE, and xenobiotics. The
72 combination of iron-mediated oxidative damage and its impaired clearance due to GSH deficiency are
73 considered in ferroptosis. Most recently, glutathione peroxidase 4 (GPx4) was identified as a key
74 inhibitor of ferroptosis[4] due to its role in reducing phospholipid hydroperoxides[5], which distinguishes it
75 from the other seven GPx family members. GPx4 uniquely interacts with oxidized phospholipids and
76 sterols *within* cell membranes for enzymatic reduction by GSH[6]. We also analyze the GSH-dependent
77 membrane repair protein peroxiredoxin 6 (Prdx6), from a different enzyme family implicated in
78 ferroptois[7]. Additionally we consider the glutathione cysteine ligase modifier (GCLM) subunit critical
79 for GSH homeostasis[8,]. While these studies have expanded the number of proteins in iron-mediated
80 oxidative and repair, other ferroptotic proteins merit consideration in future studies[8,9].

81 Iron was first linked to AD in 1953 by Louis Goodman's evidence for iron within senile plaques
82 and neurofibrils by Prussian blue histochemistry[10]. In the last two decades, associations of iron with
83 AD were strengthened by documentation of increased cerebral microbleeds and decreased blood
84 brain barrier (BBB) integrity, which increase erythrocytes in brain parenchyma. Microglial digestion of
85 intravasated blood yields hemosiderin deposits, consisting of aggregated iron and iron-containing
86 proteins[11]. The accumulation of redox active iron can result in oxidative damage with lipid
87 peroxidation, which are elevated in AD cerebrospinal fluid[12] and brain[13]. Excessive iron-mediated
88 oxidative damage is implicated in neurodegeneration and cell death. These complex iron-mediated
89 processes are commonly termed ferroptosis, and are extensively studied in cancer and other
90 diseases of aging[14].

91 While ferroptosis is implicated in AD pathology[15–17], there is limited data on human brain for
92 ferroptotic proteins[18–20] or tissue iron[18,21]. The largest study to date on AD brains showed HNE was
93 increased and varied changes in five proteins that mediate iron storage or transport[18]. This and other
94 reports are limited by the small sample size of 7 or fewer brains each, without identifying sex or ApoE
95 allele. We measured these and twenty additional proteins related to iron metabolism, antioxidants,
96 and amyloid pathology. A potential confound of prior studies is residual blood from unperfused brains.
97 Blood contains several fold higher levels of heme-iron, iron bound proteins, and GSH-utilizing
98 enzymes than brain. Experimental knockdown of GPx4 in mice caused neuron loss supporting the
99 concept of ferroptosis[22], which is cited in reviews as support for ferroptosis in AD. While GPx4 has an
100 essential role in neuronal survival, AD brains have not been examined for GPx4 or other antioxidants
101 processes relevant for ferroptosis. Moreover, xenografting human AD neurons into mice caused
102 necrotic cell death, but not apoptosis or ferroptosis[23], while a murine model of acute kidney disease
103 intertwinement of necroptosis and ferroptosis[24]. The mechanisms linking specific cell death processes
104 during AD needs further clarification.

105 To further resolve the role of iron in AD, we comprehensively examined human postmortem
106 tissue for proteins implicated in initiation or inhibition of ferroptosis. A large set of brains from
107 cognitively normal and AD was examined with equal sex and known Apolipoprotein E (ApoE) alleles.
108 The prefrontal cortex was compare with the 'AD resistant' cerebellum[25] for multiple proteins of iron
109 metabolism and antioxidant defense. The lipid raft microdomain, where the bulk of amyloid precursor
110 protein (APP) is processed for β-amyloid (Aβ) peptides, was analyzed for pathways relevant to
111 ferroptosis. We tested iron dependent mechanisms in a mouse model of AD by chelation with
112 deferoxamine (DFO) used in clinical trials for AD[26]. These findings document the loss of antioxidant
113 enzymes in lipid rafts and associated increases in lipid peroxidation.
114

RESULTS:

Minimization of residual blood in postmortem brain

Studies of iron in postmortem tissues contain intravascular blood, rich in iron proteins. In rodent studies, blood can be removed by cardiac perfusion with heparinized saline, which we show decreased heme iron in the cerebral cortex by 35% (**Table 1A**). Because perfusion is not feasible for thawed human cerebral cortex, we developed a washing procedure to minimize adherent and entrapped vascular blood. Thawed brain was minced into 2 mm cubes, followed by gentle washing with isotonic buffer (PBS). 'Washed' tissues had 65% less heme than the non-perfused, displaying less heme even when compared to perfused samples which were not washed (**Table 1A)** suggesting most heme is from residual blood on tissue rather than in the vasculature.

For human cortex (**Table 1B)** washing decreased levels of heme by 50%. As expected, washing reduced total iron levels significantly in the cortex (**Table 1B, Fig. S1A**). Importantly, total iron levels in unwashed samples were similar to those in previous studies with an increase observed with AD, suggesting that iron in previous reports[18,21,27] were possibly influenced by residual blood. Total aluminum, copper, and zinc, which generally have low levels in the blood, were not altered by washing (**Fig. S1B-D**), supporting that our washing protocol was specific to removing blood.

We further validated our washing protocol by centrifugation of the residual PBS was from tissues. The remaining supernate contained heme levels equivalent to the difference between washed and unwashed tissue (**Fig. S2A**). Serial washes were performed which showed diminishing decreases in heme concentrations after the second wash (**Fig. S2B**), for these reasons tissues were washed twice for the remaining measurements. a-hemoglobin and ferritin light chain, other markers for erythrocytes, all of which showed decreased levels greater than 50% in our washed samples (**Fig. S2C-F**). While our data suggest that some residual blood still exists in samples after washing, our protocols eliminated blood contaminants by half. Therefore, for the entirety of this study, all analyses were performed on washed samples to eliminate this confounding variable.

Table 1 Heme and Iron content of prefrontal cortex

A. Mouse, wildtype

	Non-perfused	**Perfused PBS**	**Perfused PBS + Heparin**	**Non-Perfused + Washed**
Heme/mg wet brain	3.1 ± 0.2	2.1 ± 0.2* (-32%)	2.0 ± 2.3** (-35%)	1.3 ± 0.2*** (-68%)

B. Human

Source	**Unwashed**	**Washed**
Total iron, ug/g wet brain	45 ± 4.9	26 ± 1.4 ****, -45%
Ayton et al. 2021[21]	~55	N/A
Ashraf et al. 2020[18]	~290	N/A
Heme/mg	7.1 ± 0.4	3.6 ± 0.2, ****, -50%
a-Hemoglobin, ug/mg	1,644 ± 131	815 ± 61, ****, -50%
Ferritin light chain (RFUs)	235 ± 17	100 ± 9, **** -60%

C. Sources of Iron and Ferritin

Compartment	**Total iron**	**Ferritin**
Brain, unwashed	50 ug/g wet brain	0.135 ug/g
Blood	3,500 ug/mL	3.8-14 ug/mL
Serum	1.3 ± 0.14 ug/mL	0.011-3.4 ug/mL
CSF	0.061 ± 0.006 ug/mL	0.012 ug/mL

Table 1: Heme and total iron in prefrontal cortex were assayed for effects of washing to minimize residual intravascular blood. **A**) mouse (C57BL/6J, 6 mo; n=5-6); **B**) human (AD;

n=24) and controls (65+ years; n=24) prefrontal cortex (Brodmann regions 8-10); **C)** Iron[21,28,29] and ferritin[29–31] in brain, blood, serum, and CSF. The ferritin complex in erythrocytes and tissue include FTL and FTH1. Isotonic phosphate buffered saline (PBS; pH 7.4) was used for aortic perfusion of mouse and for washing of minced mouse and human brain. 30mg prefrontal cortex was minced into 2 mm cubes and 'washed' by gentle vortexing in PBS. Heme and α-hemoglobin per mg tissue were assayed spectrophometrically relative to unwashed brain (**Fig. S3**). Total iron levels from Ashraf[33] were estimated as Fe/g protein, assuming 1 g protein/12 g wet weight brain. Brain iron and ferritin by compartment for human are >95% below blood levels, assuming 1 ml volume is equivalent to 1-gram wet brain. Significance by one way ANOVA (mouse) with Tukey's posthoc, or 2-tailed t-test (human): *p<0.05, **p<0.01, ***p<0.001, ****p<0.0001.

Lipid peroxidation increased in AD

First, we measured levels of lipid peroxidation, the oxidation of lipids by free radicals (**Fig. 1A**), previously shown in other AD tissues[34] which are a main component of ferroptosis. Oxidative damage was assessed in the prefrontal cortex with two protein adducts, HNE and 3-nitrotyrosine (NT). AD samples exhibited a significant increase in both HNE and NT compared to controls (**Fig. 1B-C**), suggesting increased lipid peroxidation is correlated with AD pathology. To determine whether these changes were associated with ApoE status or sex, we next measured HNE and NT in ApoE3 vs. ApoE4 carriers and found that lipid peroxidation was higher in ApoE4 carriers, consistent with previous reports that ApoE4 carriers are at higher risk for pathology (**Fig. 1D**). When separated by sex, females displayed an increase in HNE, but males only showed a trend, but not significant, increase in HNE, also consistent with previous reports that females display worse AD pathology than males[35] (**Fig. 1E**).

Next, we examined changes in lipid peroxidation by brain region. First, we confirmed that like cortex samples, washed cerebellum only displayed a mild increase in heme when comparing AD to control samples (**Extended Data Fig. 1A**). Cerebellum samples did display increased HNE with AD compared to control, although to a lesser extent than in the cortex (**Extended Data Fig. 1B**). In addition, no difference was observed in NT when comparing AD to control samples in the cerebellum, although cortex samples do show a difference in NT between AD and control (**Extended Data Fig. 1C**). The most striking was the loss of association of ApoE status on lipid peroxidation in the cerebellum (**Extended Data Fig. 1D**), and the reversal of association of sex: males displayed higher levels of lipid peroxidation in AD samples, whereas no difference was seen in females in the cerebellum (**Extended Data Fig. 1E**). Finally, to confirm that changes in lipid peroxidation correlate with "canonical" markers for AD pathology, we confirmed that our AD cortex and cerebellum samples display an increase in Aβ fibrils (**Extended Data Fig. 1F**) Altogether, these data suggest that the increased lipid peroxidation is associated with fibrillar amyloid. In addition, although the cerebellum does have milder AD pathology compared to the cortex in terms of lipid peroxidation, they are not completely devoid of pathology. Importantly, the association of ApoE status and sex on lipid peroxidation seems to be brain-region specific.

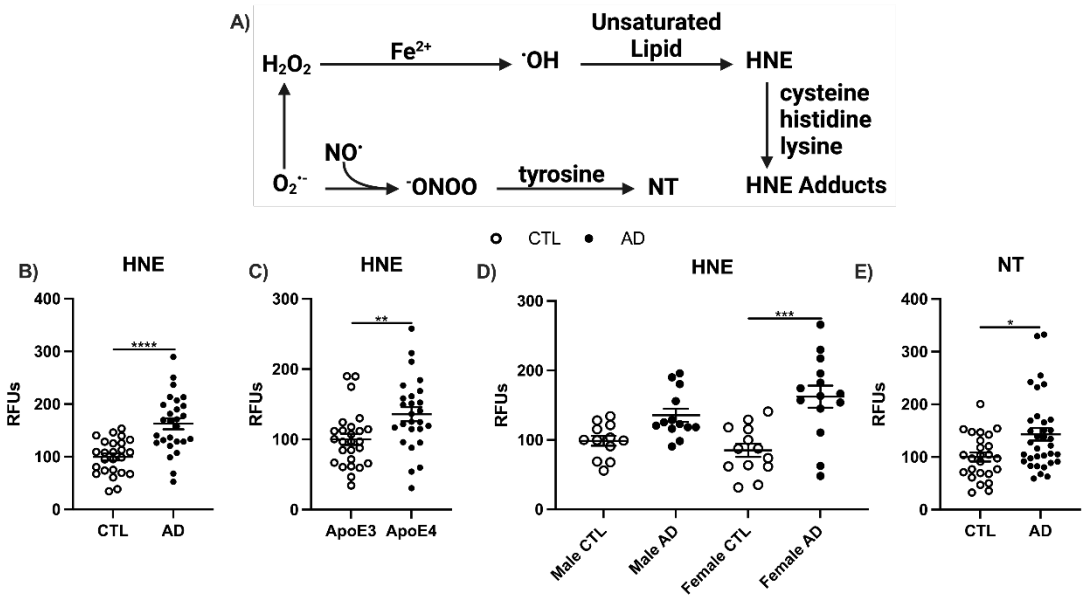

Figure 1: Oxidative damage (HNE, NT) to prefrontal cortex from age matched AD (n=27) and cognitively normal controls (CTL; n=25). **A)** Schematic representing oxidative damage to lipids and proteins. Hydroxyl radicals (·OH) are produced during oxidation of Fe^{2+} or Cu^{2+} ('Fenton chemistry') and may oxidize adjacent proteins, lipids, or nucleic acids. HNE can alter proteins via Michael addition products through its double-bonded carbons, or by forming Schiff bases through its aldehyde moiety. The bottom line shows the iron-independent oxidative pathway to form peroxynitrite $^{-}$ONOO from $O_2^{\bullet-}$ and ·NO, which can then oxidize tyrosine to NT. Aggregated human Aβ42 stimulated formation of peroxynitrite which is neurotoxic in vitro[36]. Non-heme iron also mediates lipoxygenase activity[37]. Dot blots as relative fluorescent units (RFUs) for HNE presented as **B)** cognitively normal vs AD, **C)** ApoE allele, or **D)** sex and **E)** NT. Significance, 2-tailed t-test (B-C, E), one-way ANOVA with Tukey's posthoc test (D): *p<0.05, **p<0.01, ***p<0.001, ****p<0.0001.

Iron protein metabolism is decreased in AD

While washed brain tissues did not have increases in total iron, many studies have shown that there is increased infiltration of blood cells into the brain during progression of AD due to microbleeds and loss of BBB integrity. Thus, although for biochemical assays, it is important to remove blood to differentiate between contribution of iron and iron-related factors in the blood vs. brain tissue, it is important to remember that in the context of an intact human brain, blood-contribution of iron is still an important driver in pathology. Therefore, we next sought to determine the changes in iron metabolism in AD brains, which could be driven by blood cell infiltration. Brain cellular iron is imported by the divalent metal transporter 1 (DMT1) together with transferrin (TF) and its receptor TfR. The levels of TF and TfR differ by cell type[19]. Heme iron is imported by heme carrier protein 1 (HCP1) and degraded by hemeoxygenases (HMOX1 or HMOX 2). Intracellular ferric iron is stored in complex with ferritin light chain (FTL) after oxidation of ferrous iron (Fe^{2+}) by ferritin heavy chain (FTH1). Export of ferrous iron is mediated by ferroportin (FPN).

As expected, we saw that numerous proteins involved in iron were depleted in AD brains. First, iron-transport proteins TF and its receptor TfR, were decreased in AD brains compared to control (**Fig. 2A-B**). Although we did not observe a statistically significant decrease in DMT1, there is a trend for a decrease in AD brains (**Fig. 2C**), and FPN also showed significant reduction (**Fig. 2D**). Interestingly, we did not observe major differences in heme catabolism (**Fig. 2E-G**). In addition, there was a significant increase in the iron storage protein, FTL (**Fig. 2H**), although FTH1 did not show any difference between AD and control samples (**Fig. 2I**). Relationships for iron import/export include negative correlations between iron storage protein FTL with iron import receptor TfR (r=-0.30, p=0.04) and export protein by FPN (r=-0.36, p=0.01; **Fig. 2J**). ApoE4 carriers had 2-fold higher FTL than

ApoE3 in prefrontal cortex (**TableS3**). Interestingly, AD cerebellum had dramatically different changes in iron metabolism proteins compared to the cortex. The only iron transport protein that increased in AD cerebellum compared to control samples was TF (**Extended Data Fig. 2A**), with all eithers either displaying no change or a significant decrease (**Extended Data Fig. 2B-D**). Similar to most iron transport proteins, proteins involved in heme catabolism were also largely unchanged, with only HMOX1 showing a slight decrease (**Extended Data Fig. 2E-G**). Finally, iron storage proteins also did not display any difference in AD cerebellum (**Extended Data Fig. 2H-I**).

Overall, our data show that even though total iron levels do not change in the brain, there are significant differences in proteins related to iron metabolism. These changes seem to be primarily limited to the cortex, which suggests that the cortex is more susceptible to changes to iron exposure when compared to the cerebellum.

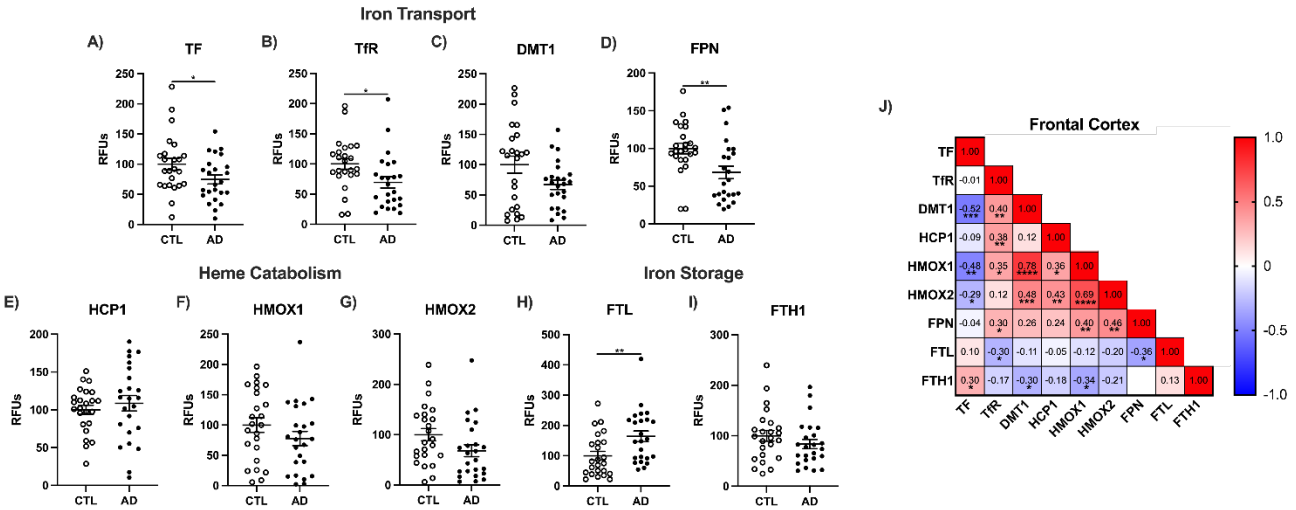

Figure 2: Iron transport and metabolism in AD prefrontal cortex (n=24) compared to cognitively normal age-matched controls (n=24). Relative fluorescent units (RFUs) from Western blots. **A)** transferrin (TF), **B)** transferrin receptor (TfR/CD71), **C**) divalent metal transporter 1 (DMT1), **D)** ferroportin (FPN), **E)** heme carrier protein 1 (HCP1), **F)** hemeoxygenase 1 (HMOX1), **G)** heme oxygenase 2 (HMOX2), **H)** ferritin light chain (FTL), **I)** ferritin heavy chain 1 (FTH1), **J)** Correlation matrix for iron metabolism in clinical AD. Significance, 2-tailed t-test (A-I), Spearman correlation (J): *p<0.05, **p<0.01, ***p<0.001, ****p<0.0001.

GSH synthesis is decreased with AD

Lipid peroxidation is driven by the loss of redox homeostasis. The tripeptide GSH conjugates to HNE for removal by several enzymes. GSH is also essential to reduce peroxides by the GPx enzyme and Prdx families. GPx4 and Prdx6 are the only known lipid hydroperoxidases capable of reducing oxidized phospholipids. These enzymes are critical in safeguarding against lipid peroxidation and ferroptosis. All other GPx family members also detoxify hydroperoxides using GSH, with GPx1 being the most abundant GPx family member in brain[38]. Shockingly, we saw an increase in GPx4 levels in AD prefrontal cortex when compared with controls (**Fig. 3A**). However, total GPx4 activity was not changed (**Fig. 3B**), suggesting that although enzyme levels may be higher, the functional output of these hydroperoxidases are unchanged. In addition, GPx1 levels and activity, as well as levels of Prdx6 were unchanged in the AD cortex (**Fig. 3C-E**). Finally, ferroptosis suppressor protein 1 (FSP1), which also protects against lipid peroxidation through the quinol cycle in a GSH-independent manner did show a significant reduction in the AD cortex (**Fig. 3F**).

To address the discrepancy between increased lipid peroxidation observed in AD brains and the lack of changes seen in detoxification enzymes, we next sought to determine whether there were defects in enzymes involved in GSH synthesis (**Fig. 3I**). The glutathione S-transferases (GST) conjugates GSH with diverse metabolites and xenobiotics. Biosynthesis of GSH depends on cystine

import via the proteins xCT (SLC7A11) and LAT1 (SLC3A2/CD98). Imported cystine is rapidly reduced to cysteine by the intracellular reducing environment[3]. The rate limiting step in GSH synthesis[39] is formation of γ-glutamylcysteine, catalyzed by glutamate cysteine ligase, with two subunits GCLC (catalytic) and GCLM (modulatory); the binding of GCLM to GCLC accelerates GSH synthesis four-fold. Next, GSH forms from addition of glycine to γ-glutamylcysteine by glutathione synthetase (GSS). Since GPx4 and Prdx6 activities are dependent on GSH, a decreased total pool of GSH would also increase lipid peroxidation, even if GPx4 and Prdx6 protein levels remain unchanged. GSH itself could not be measured due to its rapid oxidation upon death and associated artifacts, which is impossible to prevent in human postmortem tissues[40]. In the prefrontal cortex, the glutamate-cysteine ligase subunits were differentially altered by AD: the GCLM modulatory subunit was 60% lower, while GCLC the catalytic subunit was unaltered (**Fig. 3J,K**). LAT1 (L-type amino acid importer transporter) increased 33% in AD, while xCT did not differ, contrary to the 20% increase reported by Ashraf *et al.* 2020[18] (**Fig. 3L,M**). Two enzymes of the GSH cycle were not altered in AD cortex: GSS, the final step in GSH synthesis (**Fig. 3N**) and glutathione reductase (GSR) (**Fig. 3O**), which utilizes NADPH to reduce glutathione disulfide back to GSH.

Related metabolic cycles also showed selective AD changes. For the pentose phosphate pathway, G6PD was decreased by 45% in AD relative to controls, while phosphogluconate dehydrogenase (PGD) was unchanged (**Fig. 3P,Q**). These enzymes oxidize glucose to generate NAPDH required by GSR for oxidized GSH reduction (GSSG). Two groups of enzymes had correlated levels: G6PD and PGD for NADPH-production were positively correlated with GSR (both $r=0.31$, $p=0.03$), as were the amino acid importer LAT1 and cystine importer xCT ($r=0.49$, $p<0.001$; not shown)**.** Collectively, the decreases in GCLM and G6PD in the AD prefrontal cortex suggest reduced GSH levels, which contributes to the increased lipid peroxidation, despite a lack of change in GPx4 or antioxidant enzymes.

Unlike the cortex, AD cerebellum showed more changes to lipid hydroperoxidases. GPx4 levels decreased in AD cerebellum (**Extended Data Fig. 3A**), although total activity of GPx4 was unchanged (**Extended Data Fig. 3B**). In addition, although GPx1 levels and activity were unchanged like AD cortex (**Extended Data Fig. 3C-D**), Prdx6 levels were lower in AD cerebellum (**Extended Data Fig. 3E**). Finally, consistent with changes in AD cortex, FSP1 levels were also decreased in AD cerebellum (**Extended Data Fig. 3F**). Overall, AD cerebellum displayed more changes antioxidant enzymes compared to the cortex, in addition to showing a similar decrease in the GSH synthesis enzyme, GCLM (**Extended Data Fig. 3J**). Although other GSH synthesis enzymes were largely unchanged, apart from GSS which increased in the cerebellum (**Extended Data Fig. 3K-Q**).

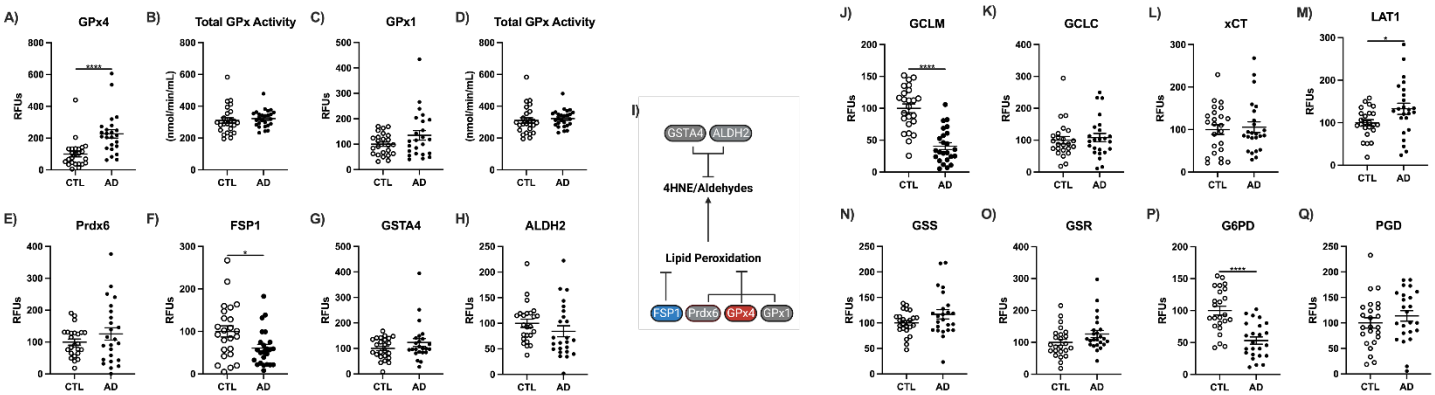

Figure 3: Enzymes that repair or mitigate lipid peroxidation and facilitate GSH production. Human prefrontal cortex Western blots and enzymatic activity in whole tissue lysate for **A)** GPx4, **B)** GPx4 activity, **C)** GPx1, **D)** total GPx activity, **E)** Prdx6, **F)** FSP1, **G)** GSTA4, and **H)** ALDH2. **I)** Schema of enzymatic repair of lipid peroxidation. GSH cycle enzyme levels by Western blots: **J)** GCLM, **K)** GCLC, **L)** xCT/SLC7A11, **M)** LAT1, **N)** GSS, **O)** GSR, **P)** G6PD, and **Q)** PGD. Significance, 2-tailed t-test (A-H, J-Q): *$p<0.05$, ****$p<0.0001$.

Lipid peroxidation in lipid rafts is increased and antioxidant defense is diminished in AD

Since measurements of whole-cell protein levels of antioxidant defense enzymes were inconclusive, we next examined the local environment of subcellular lipid rafts (**Fig. 4A**), the hub of signal transduction and where APP is processed. Lipid raft isolations were verified and compared with traditional ultracentrifugation methods[41]. First, we characterized which of the eight GPx isoforms are present in lipid rafts and detected only GPx4 and GPx1 (**Fig. S3**). Prdx6 was not detected. AD lipid rafts had significantly lower levels of the membrane protective enzymes GPx4 and GPx1, as well as decreased activity of both GPx4 and GPx1 (**Fig. 4B-E**). In addition, we observed lower levels of ALDH2 which clears free HNE and the Aβ clearance proteins, ApoE and LRP1 in AD lipid rafts (**Fig. 4F-H**). Importantly, the decreases in antioxidant protection and activity in the AD cortex were further substantiated with increased lipid raft oxidation using HNE and NT (**Fig. 4I-J**), paralleling increases in total tissue (**Fig 1B-E**). This increase in lipid peroxidation is associated with the ApoE4 allele, which exhibited higher levels of HNE in lipid rafts (**Fig. 4K**) but had no associations with sex as both males and females showed similar increases (**Fig. 4L**). Overall, these data suggest that measurements of oxidative stress, particularly linking changes to antioxidant defense and lipid peroxidation, are most robust in the lipid rafts for AD samples. Collectively, our data strongly correlate the loss of antioxidant enzymes in rafts with lipid oxidative damage in AD cortex.

Next, we performed similar lipid raft measurements in the cerebellum and found that like the AD cortex, AD cerebellum exhibited a significant decrease in GPx4 and GPx1 levels. However, unlike the cortex, GPx4 and GPx1 activity were not decreased in AD cerebellum (**Extended Data Fig. 4A-E**). Although ALDH2 levels were unchanged, ApoE and LRP1 were significantly decreased in AD cerebellum (**Extended Data Fig. 4F-H**). Similar to what was observed in whole-cell lipid peroxidation, AD cerebellum lipid rafts displayed no change in NT, but higher levels of HNE, which is consistent with our previous conclusion that in regard to lipid peroxidation, cerebellum samples display lower AD pathology than the cortex. Similar to the cortex, the cerebellum also showed higher lipid peroxidation in ApoE4 carriers (**Extended Data Fig. 4L**) with no observable difference between males and females (**Extended Data Fig. 4M**).

The non-raft membrane fraction from these same samples was also examined, which unexpectedly showed increased oxidative damage for NT but not HNE (**Extended Data Fig. 4N-Q**). No ApoE allele differences were observed for the non-raft membrane. Non-raft membrane GPx4 did not differ by AD (**Extended Data Fig. 4R**). GPx4 in non-membrane fraction was 50% lower below LR from the same tissues (**Extended Data Fig. 4S**), suggesting more localization of GPx4 to lipid rafts. These data suggest some membrane domains are selectively vulnerable to oxidation.

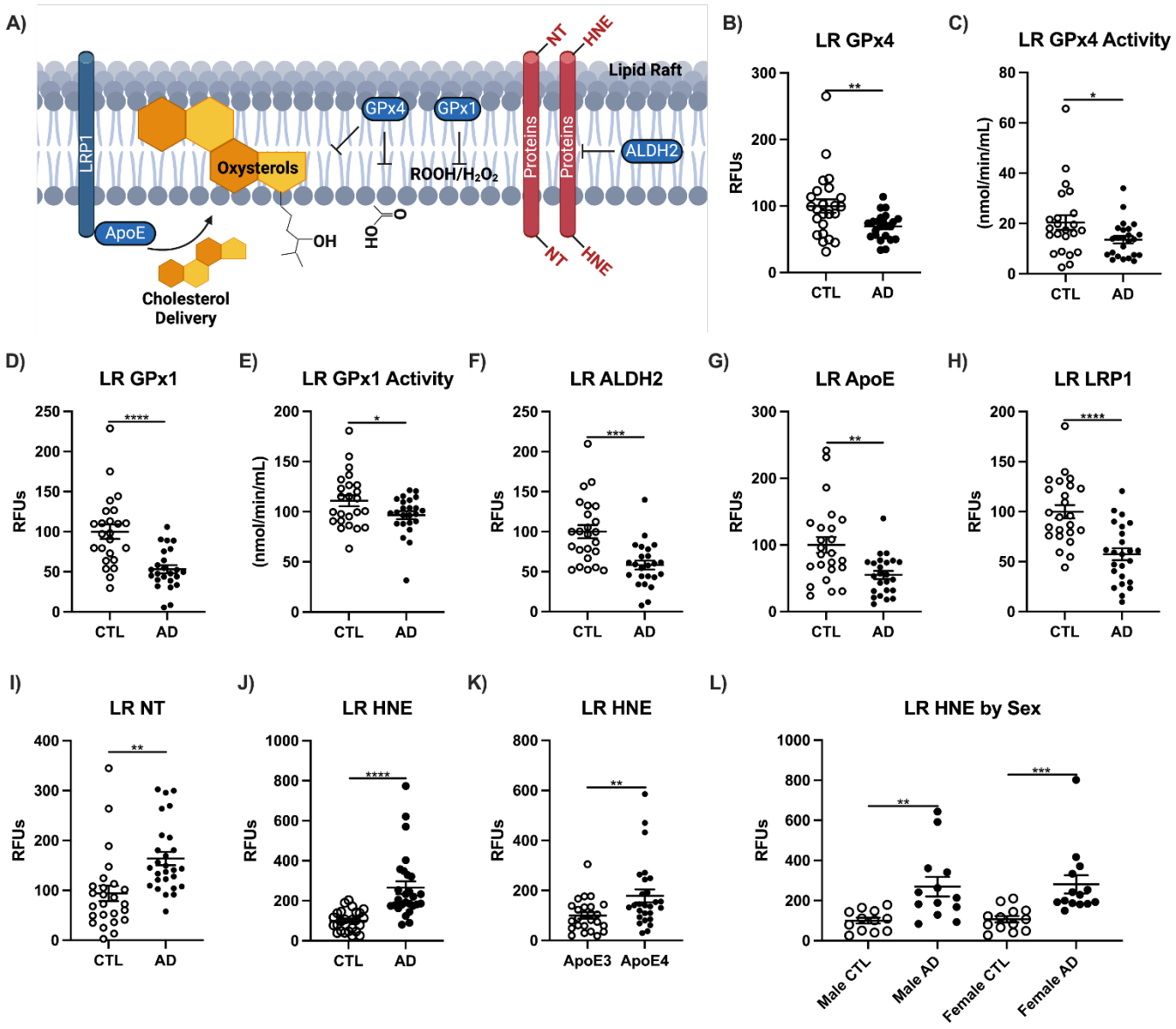

Figure 4: The lipid raft membrane fraction has increased damage and reduced antioxidant defense during AD. **A)** Schema of lipid raft damage, protective mechanisms, and cholesterol shuttling. Western blot data and enzymatic activity **B)** GPx4, **C)** GPx4 activity, **D)** GPx1, **E)** GPx1 activity, **F)** ALDH2, **G)** ApoE, **H)** LRP1. Dot blots for **I)** NT, and HNE presented as **J)** CTL vs AD, **K)** ApoE allele, and **L)** sex. Significance, by 2-tailed t-test (B-K) or one-way ANOVA with Tukey's posthoc (L): *p<0.01, **p<0.01, ***p<0.001, ****p<0.0001.

Experimental iron chelation improves pathology in AD mouse models.

Thus far, our data provides strong correlative evidence that dysfunction of iron homeostasis can drive lipid peroxidation, which is exacerbated in lipid rafts due to a loss of antioxidant enzymes in AD brains. However, one major limitation of studies with postmortem brain tissue is the inability to experimentally test causality. Therefore, we performed chelation by DFO to evaluate how removal of iron can impact AD pathology in the EFAD mouse model. DFO was chosen over other chelators because of its use in AD patients[26] and experimental studies with [H^3]DFO show it crossed the BBB, yielding 3-fold higher levels per gram in the brain than blood and kidney[42]. In our experimental paradigm, female EFAD mice received DFO in two modes: by lab chow for two weeks or by intraperitoneal injection (IP) twice daily for one week (see extended data for comparison of DFO modes).

First, we confirmed that DFO treatment ameliorated canonical markers of AD: specifically, we found that DFO-treated mice displayed a significant reduction in fibrillar Aβ (**Fig. 5A, Extended Data Fig. 5A**), and a significant increase in soluble Aβ peptides (**Fig. 5B-C, Extended Data Fig. 5B-C**). Importantly, we observed a significant reduction in lipid peroxidation using HNE in DFO-treated mice, and no change in NT which confirms the role of iron in lipid peroxidation (**Fig. 5D-E, Extended Data Fig. 5D-E**). To confirm whether these changes were due to changes in iron handling, we next measured changes in proteins related to iron metabolism. Indeed, we found that many iron transport proteins and iron storage proteins were significantly increased, although no significant changes were seen in heme catabolism proteins (**Fig. 5F-M, Extended Data Fig. 5F-M**).

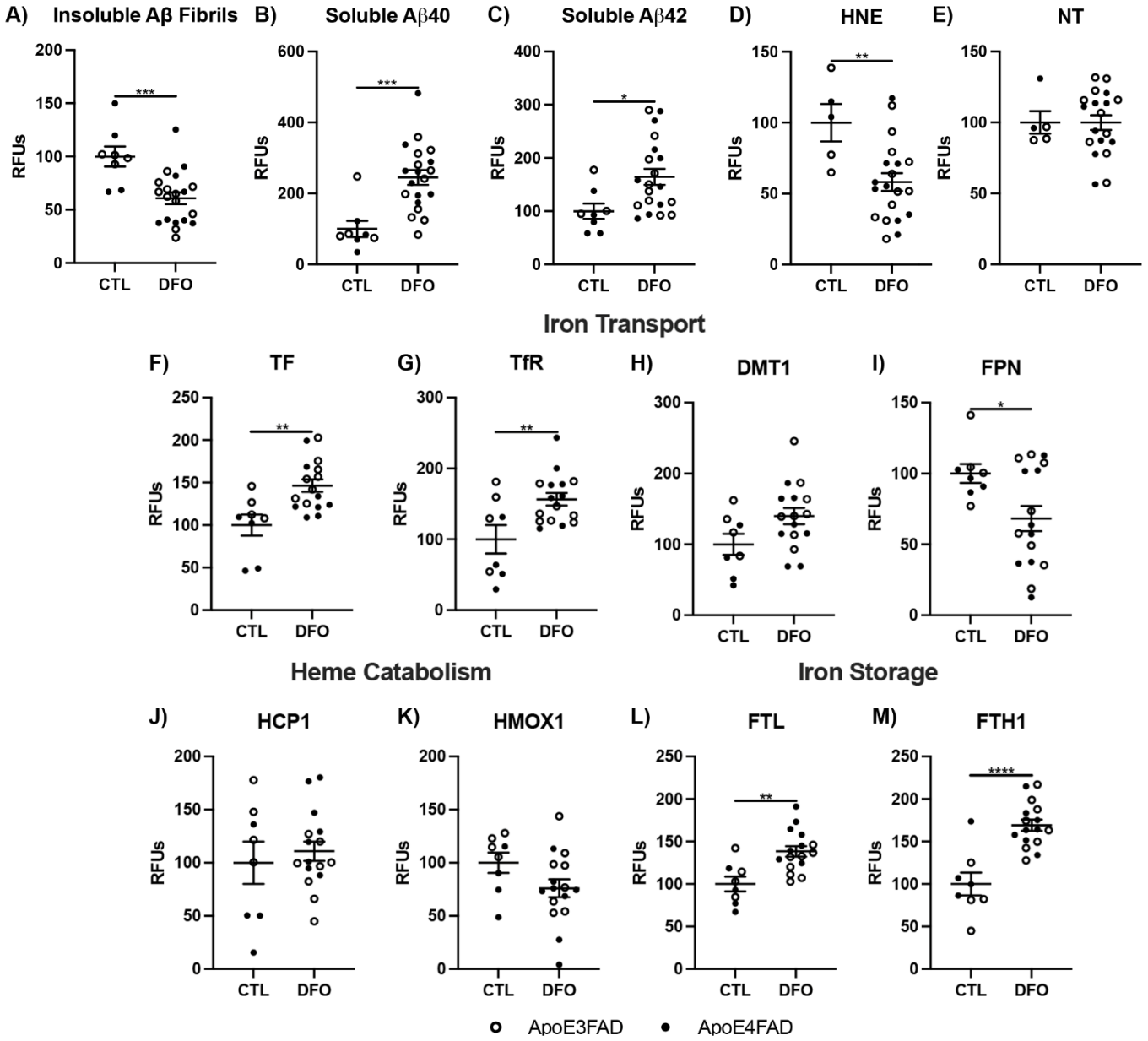

Figure 5: DFO chelation of EFAD mouse cortex: **A)** insoluble Aβ fibrils, **B)** soluble Aβ40, **C)** soluble Aβ42, **D)** HNE, **E)** NT, **F)** TF, **G)** TfR, **H)** DMT1, **I)** FPN, **J)** HCP1, **K)** HMOX1, **L)** FTL, and **M)** FTH1. Significance, 2-tailed t-test: *p<0.05, **p<0.01, ***p<0.001, ****p<0.0001.

As previously mentioned, since ferroptosis is induced by a combination of iron overload and/or an increase in oxidative damage, we next measured whether iron chelation through DFO was sufficient to improve redox handling and antioxidant activity in the brain. DFO-treatment resulted in a

significant increase in GPx4 and GPx1 levels, with a significant increase in GPx1 activity, but not GPx4 activity, although a trend of increase was seen for GPx4 activity in some animals (**Fig. 6A-D, Extended Data Fig. 6A-D**). In addition, GSTA4, GCLC, and xCT showed a significant increase in DFO-treated animals, although several others (Pdrx6, FSP1, ALDH2, GCLM) showed no difference (**Fig. 6-E-K, Extended Data Fig. 6E-K**). Overall, these experimental studies provide direct evidence that removal of iron and improved iron handling can reduce oxidative damage, improve antioxidant defense, and ameliorate AD pathology.

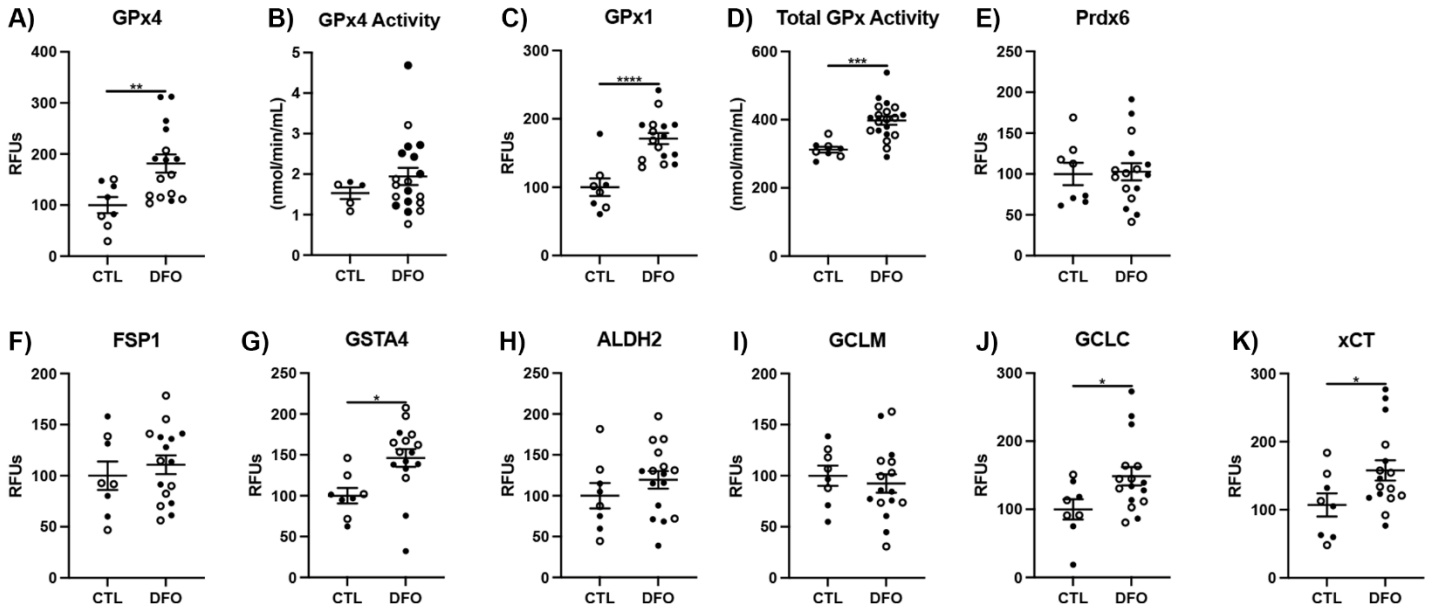

Figure 6: DFO chelation of EFAD mouse cortex. **A)** GPx4, **B)** GPx4 activity, **C)** GPx1, **D)** GPx1 activity, **E)** Prdx6, **F)** FSP1, **G)** GSTA4, **H)** ALDH2, **I)** GCLM, **J)** GCLC, **K)** xCT. Significance, 2-tailed t-test: *p<0.05, **p<0.01, ***p<0.001, ****p<0.0001.

AD pathogenesis downstream of iron-related oxidative damage is driven through changes in Nrf2 signaling.

To determine whether the outcome of iron-related oxidative damage in AD pathology was due to a dysregulation of iron homeostasis directly or through changes in downstream antioxidant pathways, we next measured changes in major transcriptional regulators of iron and oxidative damage handling. Interestingly, we found no major differences in the transcription factors, IRP1 and IRP2, involved in regulation of iron genes in the AD cortex, although a decrease in IRP2 was observed in the AD cerebellum (**Fig. S4A-C**). Importantly, we saw a significant decrease in Nrf2 in the AD cortex, one of the major transcription factors involved in antioxidant defense pathways and iron regulation (**Fig. S4D**). Interestingly, the AD cerebellum did not display a significant decrease in Nrf2. Importantly, the AD cortex also showed higher levels of NF-kB, associated with inflammation known to be elevated during AD (**Fig. S4E**). Like Nrf2, NF-kB did not show any observable differences in the cerebellum. Finally, there was a significant increase in nuclear receptor coactivator 4 (NCOA4) in the AD cortex (**Fig. S4F**) which signals for iron degradation by ferritinophagy[43]. These data were consistent with our other observations where changes in antioxidant defense pathways were more pronounced than changes in iron metabolism in the AD brain. Moreover, consistent with our previous data, the AD cortex displayed more oxidative damage than the cerebellum.

To determine whether this depletion of nuclear Nrf2 correlated with changes in gene expression of genes involved in antioxidant defense, we performed RNA-seq analysis on control-matched and case-matched AD cortex and cerebellum (**Fig. S4G-H**). Although for the purpose of this study, data were pooled into AD vs. control, we ensured that RNA-seq analysis was performed across males, females, and ApoE genotypes, which theoretically can be analyzed across sexes and

411 genotypes in a future study. GO analysis revealed that many differentially expressed genes in the AD
412 samples were those associated with numerous pathways previously implicated in AD pathology,
413 including mitochondrial dysfunction (**Fig. S4I**). Many of these significant GO terms overlapped
414 between the cortex and the cerebellum, although there were also several terms that were not shared,
415 suggesting again that the cerebellum is not fully AD resistant, although the cortex displays signs of
416 higher pathology. As expected, we did not observe major differences in gene expression of iron-
417 related genes. More importantly, we found depletion of several Nrf2 targets in the AD cortex, but not
418 in the cerebellum (**Fig. S4J**), which directly correlates with the decrease in nuclear Nrf2 found
419 specifically in the AD cortex. Transcriptome changes shared only 9 common DEGs between brain
420 regions. CD163, the hemoglobin-haptoglobin scavenger which increases in response to microbleeds
421 was shared between brain regions with AD and was among the top responding mRNAs[44]. Other
422 genes previously associated with AD or dementia were differentially expressed in both brain regions:
423 CHI3L2, FCGBP, GLI1, STAB1, APOC1, MYO7A, and long noncoding RNA JHDM1D-AS1 (**Fig.**
424 **S4K**). Taken together, our assay of transcriptional pathways supports our current hypothesis that iron
425 toxicity is directly associated with a loss of antioxidant defense in AD pathology.
426 Consistent with the human data, we also found that DFO treatment of EFAD mice did not increase
427 IRP or NOCA4 but did result in a significant increase in Nrf2 (**Fig. S4L-O**), again suggesting that most
428 pathogenic pathways downstream of iron are through changes in antioxidant defense pathways.
429
430 *Neuronal loss in AD is associated with increased ferritin, lipid peroxidation, and diminished*
431 *antioxidant defenses*
432 To next determine the physiological consequence of iron-mediated oxidative damage to lipids,
433 we measured neuronal loss in AD samples. While neuronal loss dramatically increases with
434 pathology in AD, the relationship between neuronal loss iron or membrane damage in AD is still
435 lacking. Therefore, we analyzed bulk neuronal content in prefrontal cortex and cerebellum using
436 NeuN (neuronal nuclear antigen), presynaptic SYP (synaptophysin1), and postsynaptic PSD95
437 (postsynaptic density protein 95). Strikingly, we saw a significant depletion of NeuN and PSD95, and
438 a trend for a decrease in SYP in AD cortex compared to control (**Fig. 7A-C**), although no significant
439 changes were seen for any markers in the cerebellum (**Extended Data Fig. 7A-C**). These data also
440 by Braak Score shows a similar trend whereby higher Braak scores correlated with lower NeuN and
441 PSD95 in the cortex, but not the cerebellum (**Fig. 7D-F, Extended Data Fig. D-F**). In addition,
442 neuronal markers varied inversely with cortex tissue levels of heme by Braak score, while NeuN
443 varied inversely with ferritin light chain (**Fig. 7D**). The relationship for NeuN and heme differed by
444 Braak stage, but not by clinical dementia status. These inverse associations give the first direct
445 associations of brain iron markers with brain region-specific neuron loss during AD. The inverse
446 correlation of NeuN with HNE strengthens the relationship of lipid peroxidation to neuron loss. Many
447 of these relationships were weakened or absent from cerebellum, consistent with its reduced
448 neuronal loss (**Extended Data Fig. 7D-E**). However, positive correlations between NeuN and FPN or
449 NeuN and GCLM protein levels were the only shared relationships by both criteria and in cortex and
450 cerebellum. These relationships highlight the role iron export by FPN or GSH production by GCLM for
451 neuronal survival. Overall, these data provide direct evidence that the physiological consequence of
452 increased iron-related oxidative damage results in neuronal cell death, likely through the induction of
453 ferroptosis.

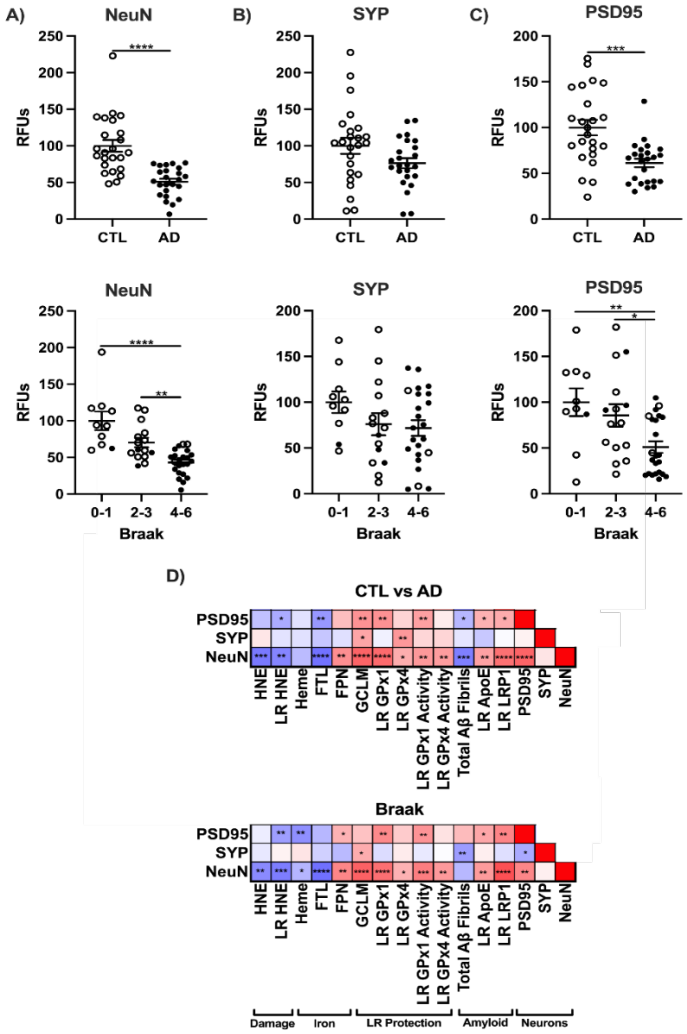

Figure 7: Neuronal loss and transcriptional changes in AD prefrontal cortex. Western blots as relative fluorescent units (RFU) of neuronal markers by CTL vs AD, or Braak stage[41]. **A)** neuronal nuclei antigen (NeuN), **B)** synaptophysin 1 (SYP), **C)** postsynaptic density protein 95 (PSD95). **D)** Correlation matrix for variables with significant relationships to NeuN by CTL vs AD or Braak. Significance, 2-tailed t-test (CTL vs AD), one-way ANOVA (Braak) with Tukey's posthoc, or Spearman correlation: *p<0.05, **p<0.01, ***p<0.001, ****p<0.0001.

ApoE allele associations with lipid rafts, lipid peroxidation, and antioxidant defense

Because ApoE4 is associated with greater AD neuropathology, we investigated where our observed changes with iron metabolism, antioxidant defense to lipid rafts, amyloid processing and clearance during AD were associated with ApoE status. Importantly, ApoE4,4 (E4,4) carriers had a significant reduction in NeuN in the cortex, suggesting greater neuronal death is correlated with E4,4 (**Fig. 8A**). Interestingly, cerebellum NeuN was also decreased in E4,4 carriers despite its reported resistance to AD (**Extended Data Fig. E8A**). In addition, we observed a significant decrease in lipid raft cholesterol and proteins in E4,4 cortex (**Fig. 8 B-D**), which suggests that composition of lipid rafts is compromised in E4,4 carriers. As expected, Aβ fibrils were increased in E4,4 cortex, although total LR APP was unaffected (**Fig. 8E-F**). The cerebellum did not display major changes in lipid raft composition across ApoE genotypes (**Extended Data Fig. 8B-E**), although Aβ fibrils were still significantly increased in E4,4, again highlighting that although many markers of pathology are not seen in the cerebellum compared to the cortex, it is not completely devoid of all pathological phenotypes.

Next, to determine the consequence of changes in the lipid raft in E4,4 carriers, we measured amyloid clearance proteins ApoE and LRP1 and saw a significant reduction in ApoE4,4 cortex and cerebellum (**Fig. 8G-H, Extended Data Fig. 8G-H**). Interestingly, the iron storage protein FTL was highest in E4,4 cortex with corresponding decreases in the iron export protein FPN (**Fig. 8I,J**). Importantly, these changes were directly paralleled with lipid peroxidation in the rafts, as HNE adducts increased significantly in E4,4 carriers (**Fig. 8K**). These changes in lipid peroxidation were also observed with corresponding loss of antioxidant capacity, as GCLM, GPx1 activity, and GPx4 levels and activity, although not GPx1 levels, were significantly reduced in E4,4 carriers (**Fig. 8L-P**). Interestingly, although some of these phenotypes were shared across brain regions, most changes were not seen in the cerebellum (**Extended Data Fig. 8I-P**). Overall, our data provide strong evidence that many phenotypes associated with iron-related oxidative damage of lipids, which drive AD pathology, are worse in the E4,4 carriers, consistent with the consensus that E4,4 carriers are at the highest risk for AD. LR markers correlated negatively with Aβ fibrils in cerebral cortex more strongly (**Fig. 8Q**) than cerebellum (**Fig. E8R**). Aβ fibrils also correlated positively with LR HNE levels. The correlation between NeuN and GCLM or FPN remained strong by ApoE allele, as well as for clinical 'CTL vs AD' and 'Braak' stage. LR GPx1 also positively correlated with NeuN.

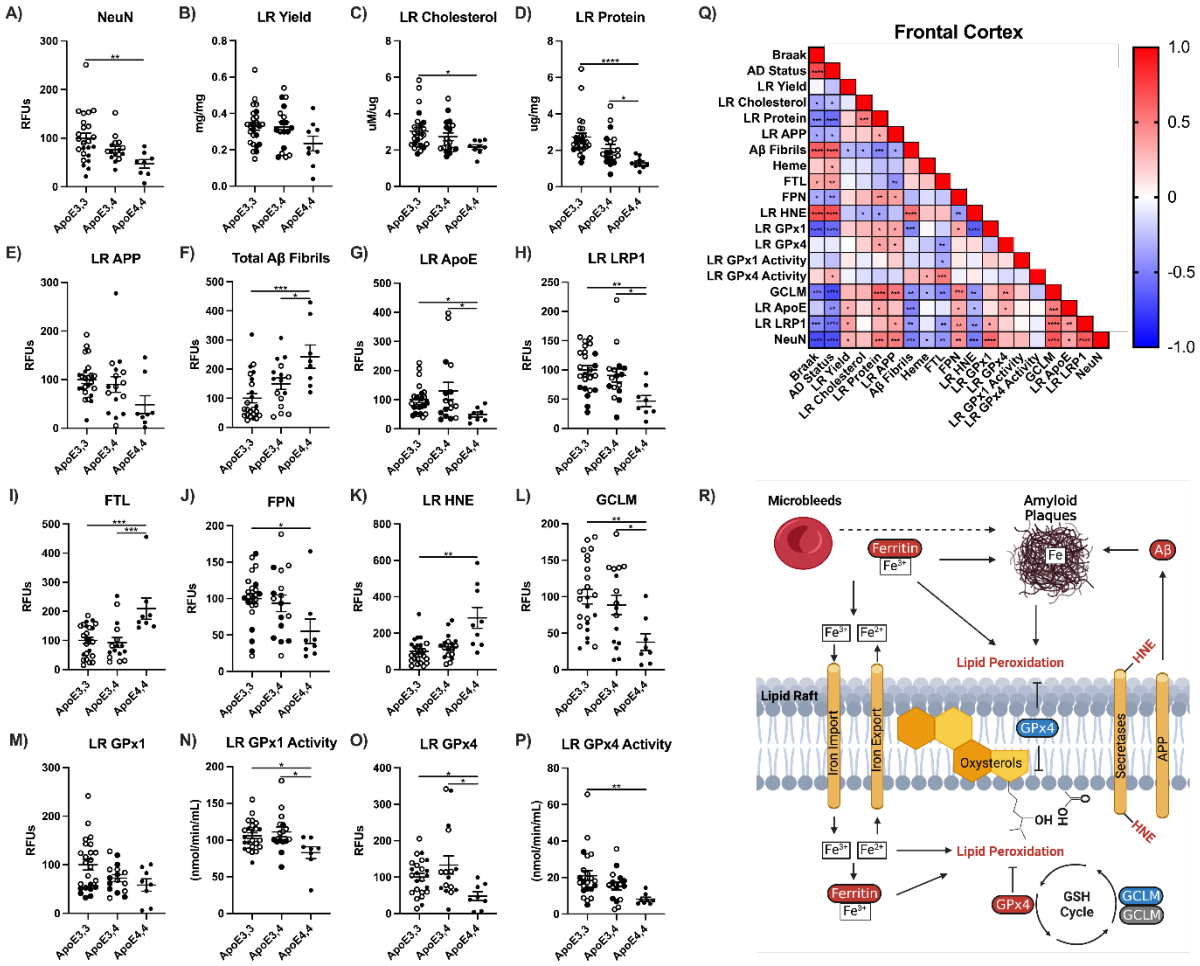

Figure 8: ApoE allele associations with lipid rafts, antioxidant defense, and amyloid in human prefrontal cortex. **A)** NeuN, **B)** LR yield, **C)** LR cholesterol, **D)** total LR protein, **E)** LR APP, **F)** total Aβ fibrils, **G)** LR ApoE, **H)** LR LRP1, **I)** FTL, **J)** FPN, **K)** LR HNE, **L)** GCLM, **M)** LR GPx1, **N)** LR GPx1 activity, **O)** LR GPx4, **P)** LR GPx4 activity. **Q)** Correlation matrix by ApoE allele. One way ANOVA by Tukey's posthoc, or Spearman correlation: *p<0.05, **p<0.01, ***p<0.001, ****p<0.0001. **R)** Model for ferroptosis in AD.

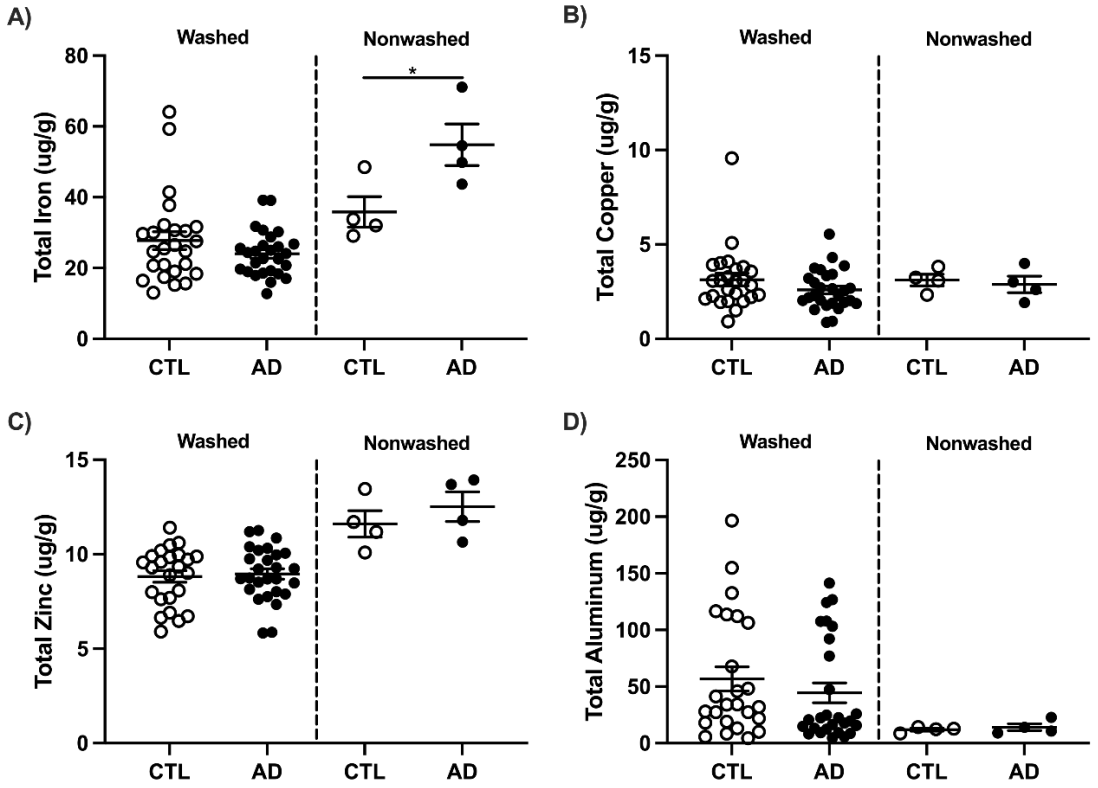

Supplemental Figure 1: Total **A)** Iron, **B)** Copper, **C)** Zinc, and **D)** Aluminum concentrations by ICP-MS (Table 1). **A-D,** Human prefrontal cortex was washed with PBS or non-washed. Significance by 2-tailed t-test (CTL vs AD): *p<0.05.

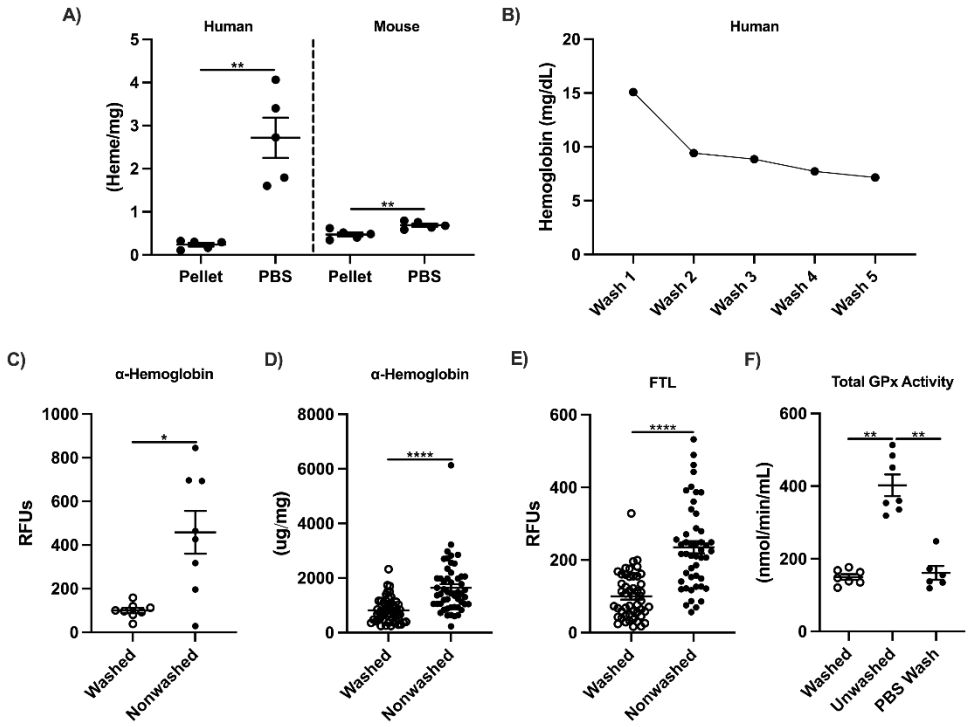

Supplemental Figure 2: Blood on tissues influences iron and antioxidant measurements. **A)** Nonperfused mouse and washed human cerebral cortex. **B)** Collected wash was assayed for heme in 5 consecutive washes; washes 1 and 2 reduced makers by 90%; washes 3-5 yielded <10% further decreases. The lower α-

hemoglobin in washed human frontal cortex was confirmed by **C)** Western blot, **D)** immunoassay, **E)** Western blot for FTL, and **F)** total GPx activity. Significance, 2-tailed t-test (A, C-E) or one-way ANOVA with Tukey's post-hoc (F): *p<0.05, **p<0.01, ***p<0.001, ****p<0.0001.

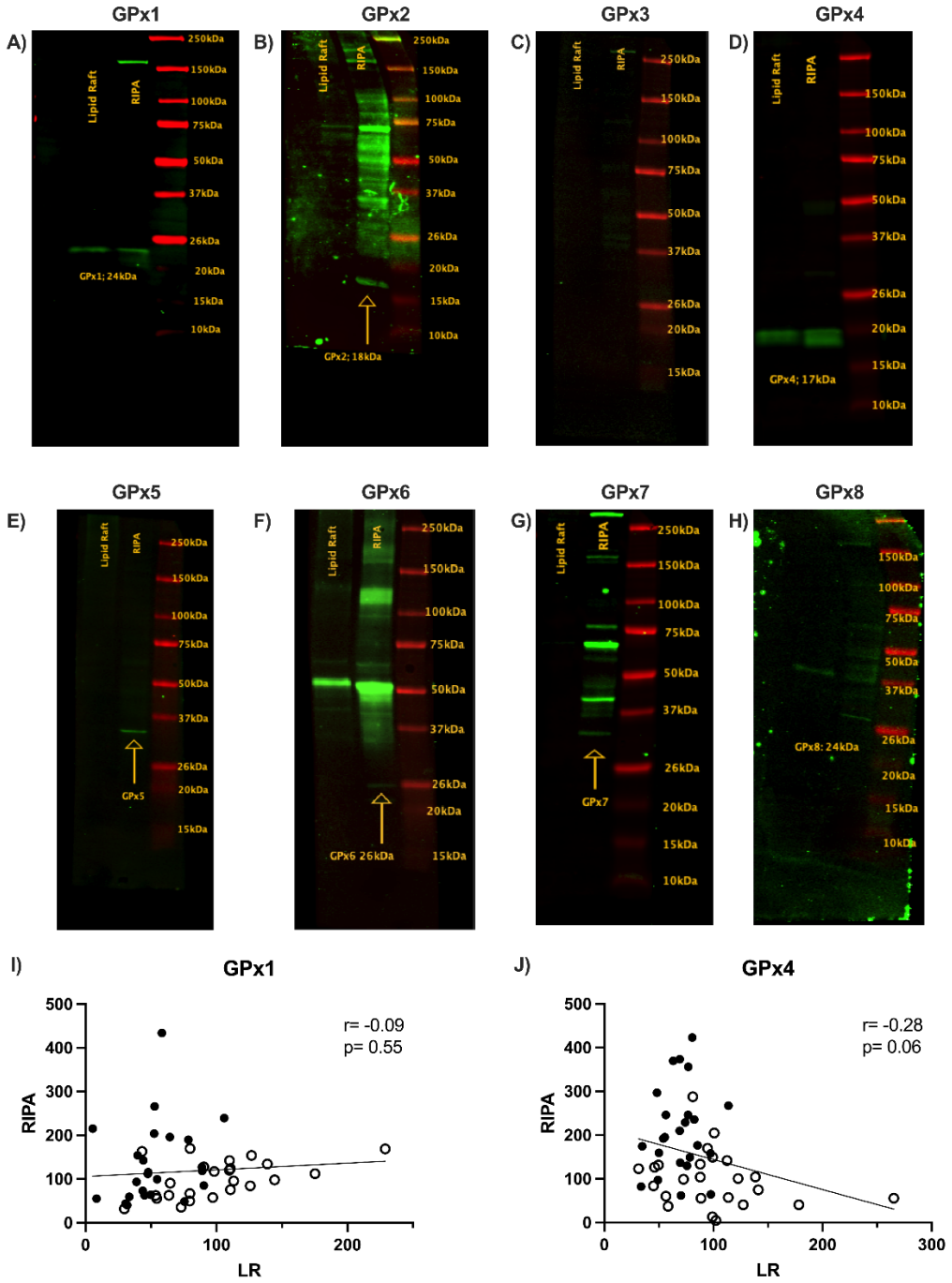

Supplemental Figure 3: Glutathione peroxidases in lipid rafts from human prefrontal cortex. The GPx isoforms were resolved immunologically on Western blots of lipid raft and whole cell lysates (RIPA buffer extract). **A)** GPx1, **B)** GPx2, **C)** GPx3, **D)** GPx4, **E)** GPx5, **F)** GPx6, **G)** GPx7, **H)** GPx8. Coplots of **I)** GPx1 and **J)** GPx4 for RIPA extract and lipid raft fractions.

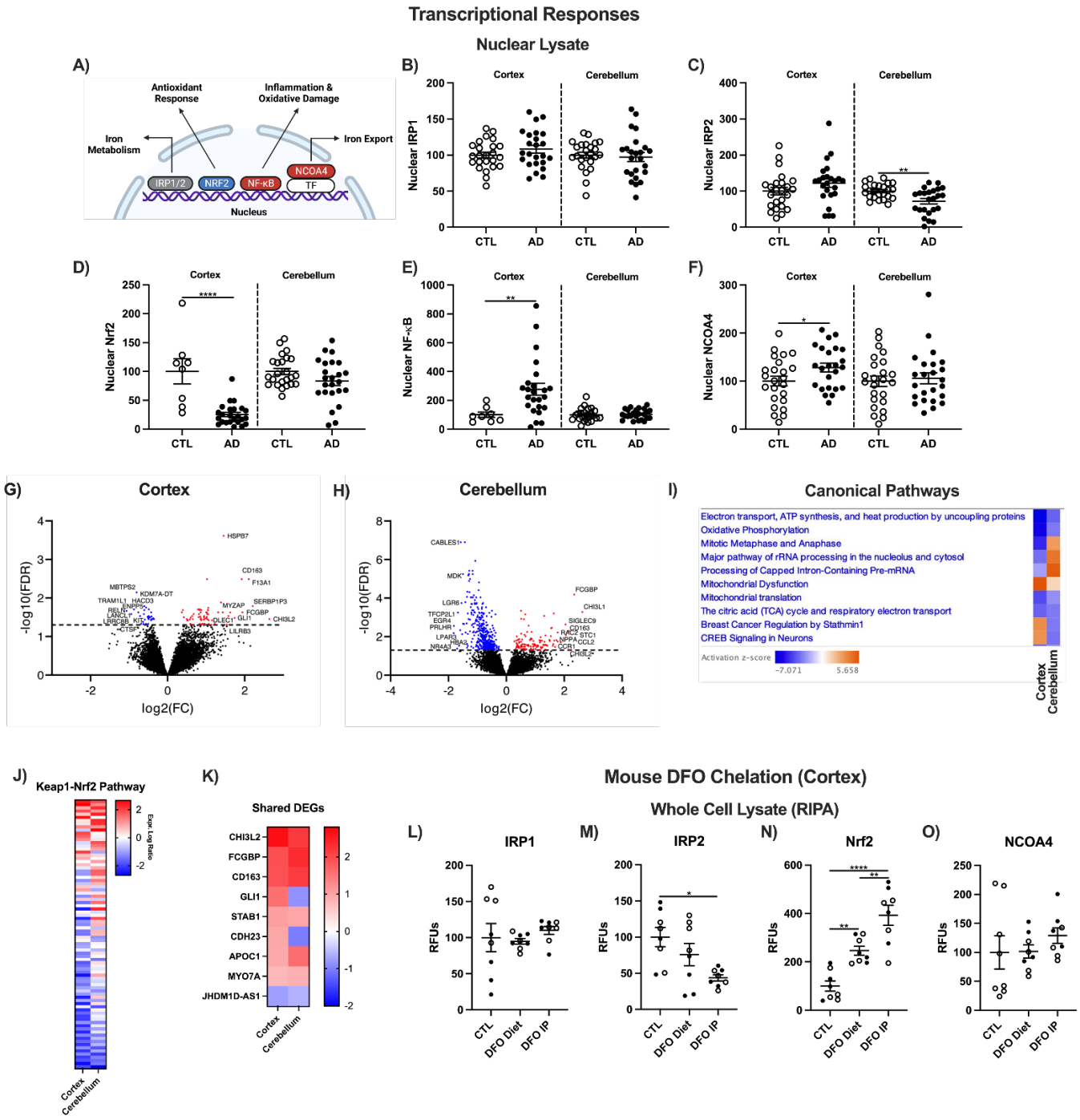

Supplemental Figure 4: Transcriptional responses mediating iron homeostasis. **A)** Transcription factors of genes for antioxidant defense and iron signaling in human prefrontal cortex of AD and CTL. IRP, iron regulatory protein; Nrf2, nuclear factor erythroid 2–related factor 2; NF-κB p65, nuclear factor κ-light-chain-enhancer of activated B cells; NCOA4, nuclear receptor coactivator 4; TF, transcription factor. Western blot data from nuclear lysates as relative fluorescent units (RFUs) for **B)** IRP1, **C)** IRP2, **D)** Nrf2, **E)** NF-κB p65, and **F)** NCOA4 in prefrontal cortex and cerebellum. Volcano plots of DEGs from RNA-seq for **G)** prefrontal cortex, **H)** cerebellum, and **I)** top shared canonical pathways. **J)** Keap1- Nrf2 pathway and **K)** shared DEGs between cortex and cerebellum. DFO treated EFAD mouse cortex total (RIPA lysate) for **L)** IRP1, **M)** IRP2, **N)** Nrf2, and **O)** NCOA4 protein in. Significance by 2-tailed t-test (B-F) or One way ANOVA with Tukey's posthoc test (L-O): *p<0.05, **p<0.01, ****p<0.0001.

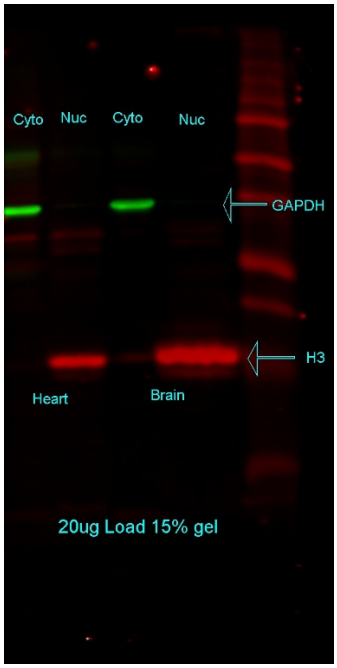

Supplemental Figure 5: Nuclear and cytosolic fractions from mouse heart and cortex. Lysates probed by Western blot for histone 3 (H3, nuclear marker) and glyceraldehyde 3-phosphate dehydrogenase (GAPDH, cytosolic marker).

Age	Sex	AD Status	Braak	ApoE Allele	PMI (hours)	Frontal Cortex	Cerebellum	MMSE	MMSE Interval (Months)	ADRC
99	Female	CTL	0	3,3	9	x	x	28	23.4	USC
91	Female	CTL	0	3,3	8.75	x	x	20	84	USC
85	Female	CTL	0	3,3	7	x	x	N/A	N/A	USC
95	Female	CTL	1	3,3	3.25	x	x	N/A	N/A	USC
87	Female	CTL	2	3,3	10.75	x	x	29	1	USC
95	Female	CTL	2	3,3	2.92	x	x	N/A	N/A	UCI
86	Female	CTL	3	3,3	6.17	x	x	30	35.5	UCI
90	Female	CTL	3	3,3	2.2	x	x	N/A	N/A	UCI
89	Female	CTL	3	3,3	3.58	x	N/A	24	5.9	UCI
94	Female	AD	4	3,3	10.5	x	x	N/A	N/A	USC
81	Female	AD	5	3,3	7.5	x	x	N/A	N/A	USC
89	Female	AD	5	3,3	1.5	x	x	N/A	N/A	USC
66	Female	AD	6	3,3	17	x	x	N/A	N/A	USC
70	Female	CTL	1	3,4	4.17	N/A	x	28	20.1	UW
86	Female	CTL	3	3,4	9.33	N/A	x	29	12.3	UW
97	Female	CTL	3	3,4	0	N/A	x	26	6.6	UW
91	Female	CTL	3	3,4	11.2	x	x	23	10.1	UW
85	Female	CTL	3	3,4	4.2	N/A	x	29	37.9	UW
89	Female	CTL	3	3,4	3.5	N/A	x	27	28.7	UW
74	Female	CTL	3	3,4	4.5	N/A	x	30	44.3	UW
91	Female	CTL	3	3,4	3.33	x	x	27	42.5	UCI
87	Female	CTL	3	3,4	4.57	x	x	29	85.6	UCI
93	Female	CTL	5	3,4	4.15	x	x	30	81.6	UCI
81	Female	AD	5	3,4	5.5	x	x	N/A	N/A	USC
84	Female	AD	5	3,4	6	x	x	N/A	N/A	USC
80	Female	AD	5	3,4	19	x	x	N/A	N/A	USC
96	Female	AD	6	3,4	9	N/A	x	N/A	N/A	USC
77	Female	AD	6	3,4	8.25	x	x	N/A	N/A	USC
87	Female	AD	6	3,4	4.5	N/A	x	N/A	N/A	USC
78	Female	AD	4	4,4	15.5	x	x	N/A	N/A	USC
81	Female	AD	5	4,4	4	x	x	N/A	N/A	USC
80	Female	AD	5	4,4	3.75	x	x	N/A	N/A	USC
76	Female	AD	5	4,4	5.25	x	x	N/A	N/A	USC
82	Male	CTL	0	3,3	9	x	x	28	N/A	USC
93	Male	CTL	0	3,3	12	x	x	30	1229.2	USC
93	Male	CTL	0	3,3	3.75	x	x	N/A	N/A	USC
76	Male	CTL	0	3,3	11.25	x	x	N/A	N/A	USC
86	Male	CTL	2	3,3	4.42	x	x	25	48.4	UCI
83	Male	CTL	2	3,3	3.18	x	x	N/A	N/A	UCI
86	Male	CTL	3	3,3	2.92	x	x	20	37	UCI
80	Male	CTL	3	3,3	4.05	x	x	26	95.1	UCI
97	Male	AD	3	3,3	5.25	x	x	N/A	N/A	USC
87	Male	AD	4	3,3	4.75	x	x	N/A	N/A	USC
76	Male	AD	5	3,3	9.75	x	x	N/A	N/A	USC
88	Male	AD	5	3,3	6.75	x	x	N/A	N/A	USC
92	Male	CTL	0	3,4	5.25	x	x	N/A	N/A	USC
87	Male	CTL	1	3,4	4	N/A	x	25	8.9	UW
90	Male	CTL	3	3,4	5.8	x	x	N/A	N/A	UCI
97	Male	CTL	4	3,4	5.83	x	x	26	7	UCI
87	Male	CTL	4	3,4	6.28	x	x	22	101.5	UCI
77	Male	AD	2	3,4	6	x	x	N/A	N/A	USC
81	Male	AD	3	3,4	7.25	x	x	N/A	N/A	USC
85	Male	AD	5	3,4	7.25	x	x	N/A	N/A	USC
72	Male	AD	6	3,4	9	x	x	N/A	N/A	USC
75	Male	AD	0	4,4	9.5	x	x	N/A	N/A	USC
88	Male	AD	5	4,4	5	x	x	N/A	N/A	USC
92	Male	AD	5	4,4	8.25	x	x	N/A	N/A	USC
70	Male	AD	5	4,4	3.5	x	x	N/A	N/A	USC
81	Male	AD	5	4,4	6.54	N/A	x	N/A	N/A	USC

Supplemental Table 1: Data shown for brain specimens by each ADRC source: USC, 37; UCI, 14; UW, 8. White, 76%; Latino, 14%; African American, 3%; Asian, 2%; N/A, 5%. ApoE3,3, 42%, ApoE3,4, 42%, ApoE4,4, 16%.

	NFT-Bearing Neurons				**NFT-Free Neurons**		
	NFT	Cytoplasm	Nucleus	Neuropil	Cytoplasm	Nucleus	Neuropil
AD	65 ± 9	20 ± 3	42 ± 5	14 ± 3	12 ± 2*	44 ± 7*	11 ± 1*
CTL	N/A	N/A	N/A	N/A	4 ± 0.5	17 ± 2	4 ± 0.5

Supplemental Table 2: Iron in NFT free and bearing neurons presented as mass charge ratio (m/z) by Good et al. 1992[45]. Significance analyzed in this report by 2-tailed t-test: *p<0.05.

Measurement	Cortex (AD vs CTL)	Cerebellum (AD vs CTL)	Cortex (ApoE3,3 vs 3,4 & 4,4)	Cerebellum (ApoE3,3 vs 3,4 & 4,4)	Cortex Male (AD vs CTL)	Cortex Female (AD vs CTL)
FTL	+65% **	+10%, n.s.	+30%, n.s.	-30%, n.s.	+55%, n.s.	+75% *
FSP1	-40% ****	-30% ****	-40% *	-20% **	-50%, n.s.	-30% *
GCLM	-60% ****	-35% *	-30%, n.s.	-15%, n.s.	-65% ****	-55% ***
GPx4	+110% ****	-15% *	+45% *	-30, n.s.	+45%, n.s.	+210% ***
GPx4, LR	-30% **	-40% ****	-5%, n.s.	-5%, n.s.	-25% **	-35%, n.s.
GPx4 Activity, LR	-40% *	-10%, n.s.	-50% **	-15%, n.s.	-40%, n.s.	-40%, n.s.
Heme	+25% *	+30% **	+5%, n.s.	+10%, n.s.	+20%, n.s.	+25%, n.s.
HNE, Total	+60% ****	-20%, n.s.	+35% **	-25% *	+35% **	+90% ***
HNE, LR	+160% ****	+45% **	+80% **	+35% *	+170% **	+180% ***
NF-κB, nuclear	+175% **	+5%, n.s.	+70%, n.s.	+5%, n.s.	+45%, n.s.	+290% **
Nrf2, nuclear	-75% ****	-15%, n.s,	-65% ***	-15%, n.s.	-85% **	-60% **

Supplemental Table 3: AD change in prefrontal cortex (Brodmann 8-10) and cerebellum by ApoE3 and 4 alleles. FTL, ferritin light chain; FSP1, ferroptosis suppressor protein 1; GPx4, glutathione peroxidase 4. t-test *p<0.05, **p<0.01, ***p<0.001, ****p<0.0001; n.s, not significant.

Extended Figures

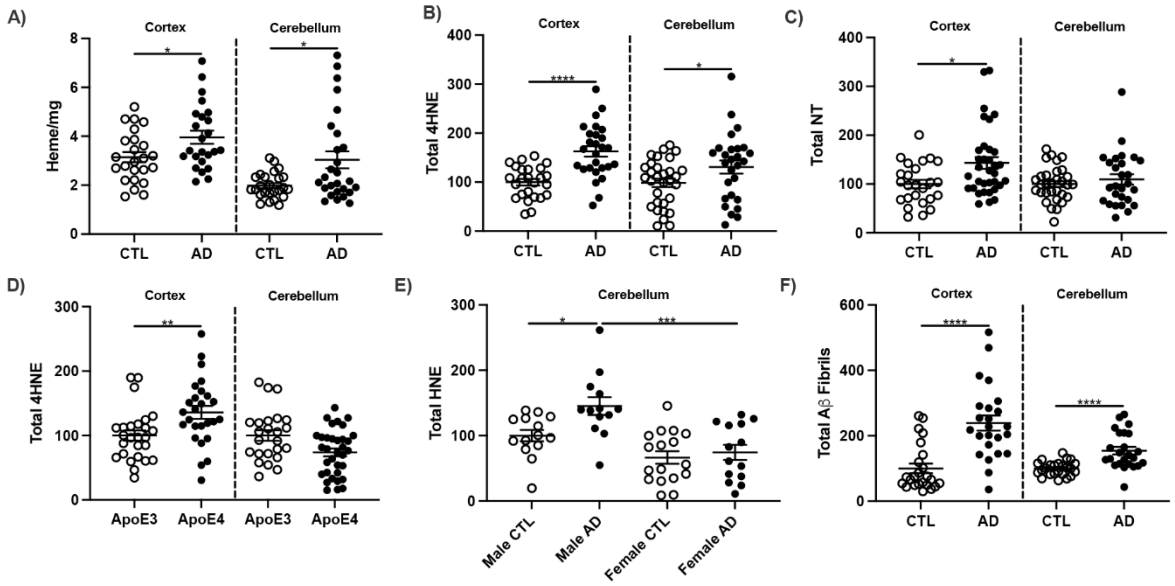

Extended data Figure 1: Oxidative damage (HNE, NT) in human prefrontal cortex and cerebellar proteins in age matched AD and cognitively normal control (CTL). Prefrontal cortex from Brodmann area 8, 9, or 10 and cerebellum were washed for measurements of **A)** heme, **B)** dot blot for 4HNE, **C)** dot blot for NT, **D)** HNE, **E)** HNE, **F)** total amyloid fibrils**.** Significance, 2-tailed t-test (A-D,F), one-way ANOVA with Tukey's posthoc test (E): *p<0.05, **p<0.01, ***p<0.001, ****p<0.0001.

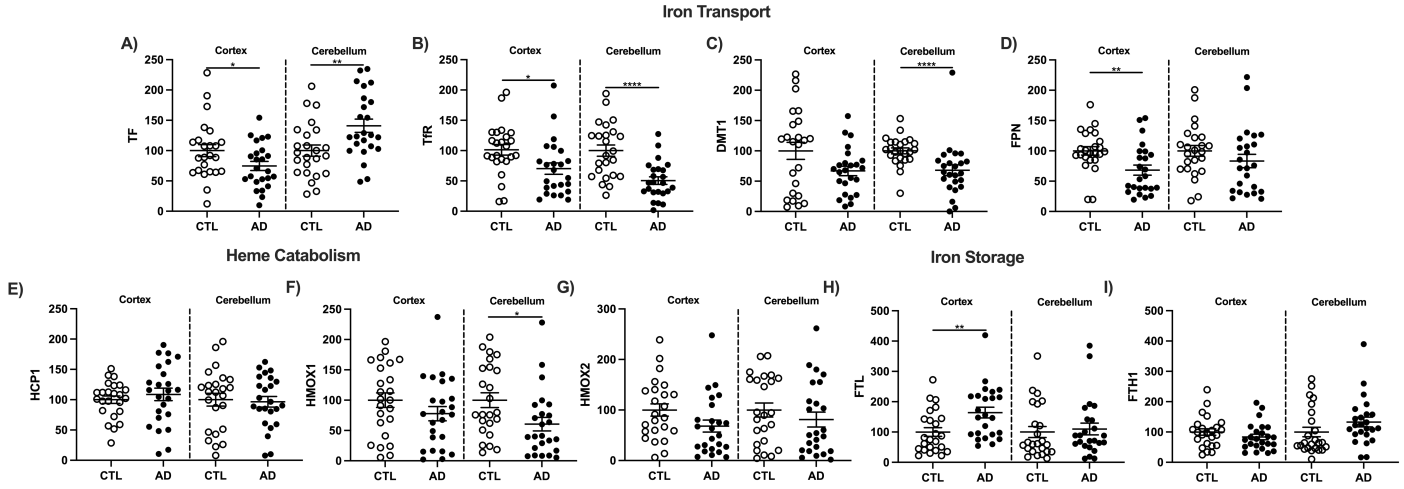

Extended Data Figure 2: Iron transport and metabolism in AD vs cognitively normal prefrontal cortex and cerebellum. Western blots data for **A)** transferrin (TF), **B)** transferrin receptor (TfR/CD71), **C**) divalent metal transporter 1 (DMT1), **D)** ferroportin (FPN), **E)**, heme carrier protein 1 (HCP1), **F)** hemeoxygenase 1 (HMOX1), **G)** heme oxygenase 2 (HMOX2), **H)** ferritin light chain (FTL), **I)** ferritin heavy chain 1 (FTH1). Significance, 2-tailed t-test (A-I): *p<0.05, **p<0.01, ****p<0.0001.

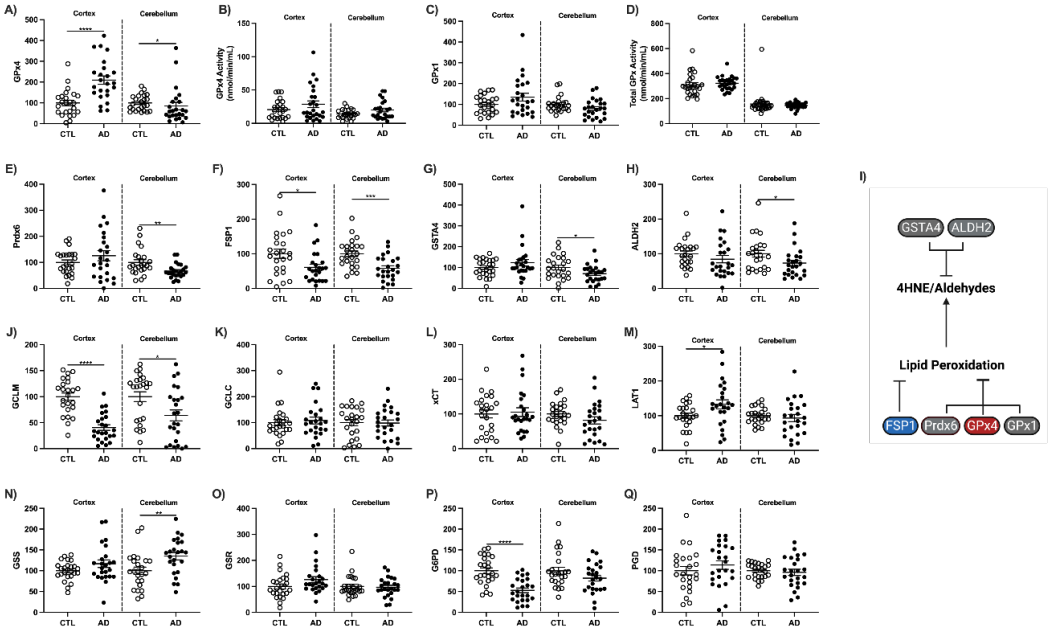

Extended Data Figure 3: Enzymes that mitigate lipid peroxidation and facilitate GSH production. Western blot or enzyme activity units for prefrontal cortex or cerebellum from whole tissue lysate for **A)** GPx4, **B)** GPx4 activity, **C)** GPx1, **D)** total GPx activity, **E)** Prdx6, **F)** FSP1, **G)** GSTA4, and **H)** ALDH2. **I)** Enzymatic repair of lipid peroxidation. GSH cycle enzyme levels by Western blots, as relative fluorescent units (RFU) **J)** GCLM, **K)** GCLC, **L)** xCT/SLC7A11, **M)** LAT1, **N)** GSS, **O)** GSR, **P)** G6PD, and **Q)** PGD. Significance, 2-tailed t-test (A-H,J-Q): *p<0.05, **p<0.01, ***p<0.001, ****p<0.0001.

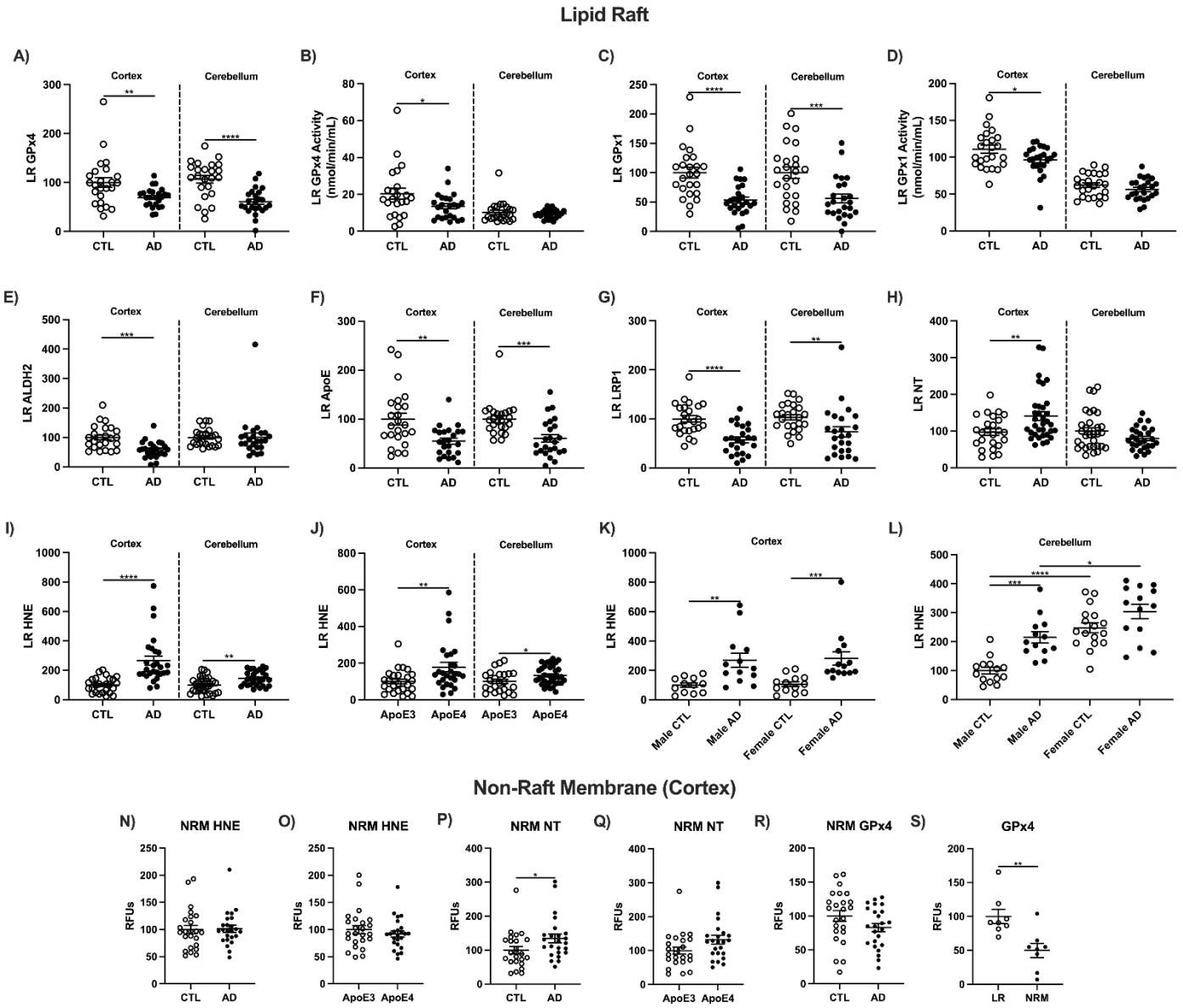

Extended Data Figure 4: The AD lipid raft has increased damage and reduced antioxidant defense. **A)** Schema of lipid raft damage, protective mechanisms, and cholesterol shuttling in AD prefrontal cortex and cerebellum. Western blots as relative fluorescent units (RFUs) or enzymatic activity **B)** GPx4, **C)** GPx4 activity **D)** GPx1, **E)** GPx1 activity, **F)** ALDH2, **G)** ApoE, **H)** LRP1. Dot blots for **I)** NT, and HNE presented as **J)** CTL vs AD, **K)** ApoE allele, and sex for **L)** cortex and **M)** cerebellum. Significance, 2-tailed t-test (A-J, N-S), one-way ANOVA with Tukey's posthoc test (K,L): *p<0.05, **p<0.01, ***p<0.001, ****p<0.0001.

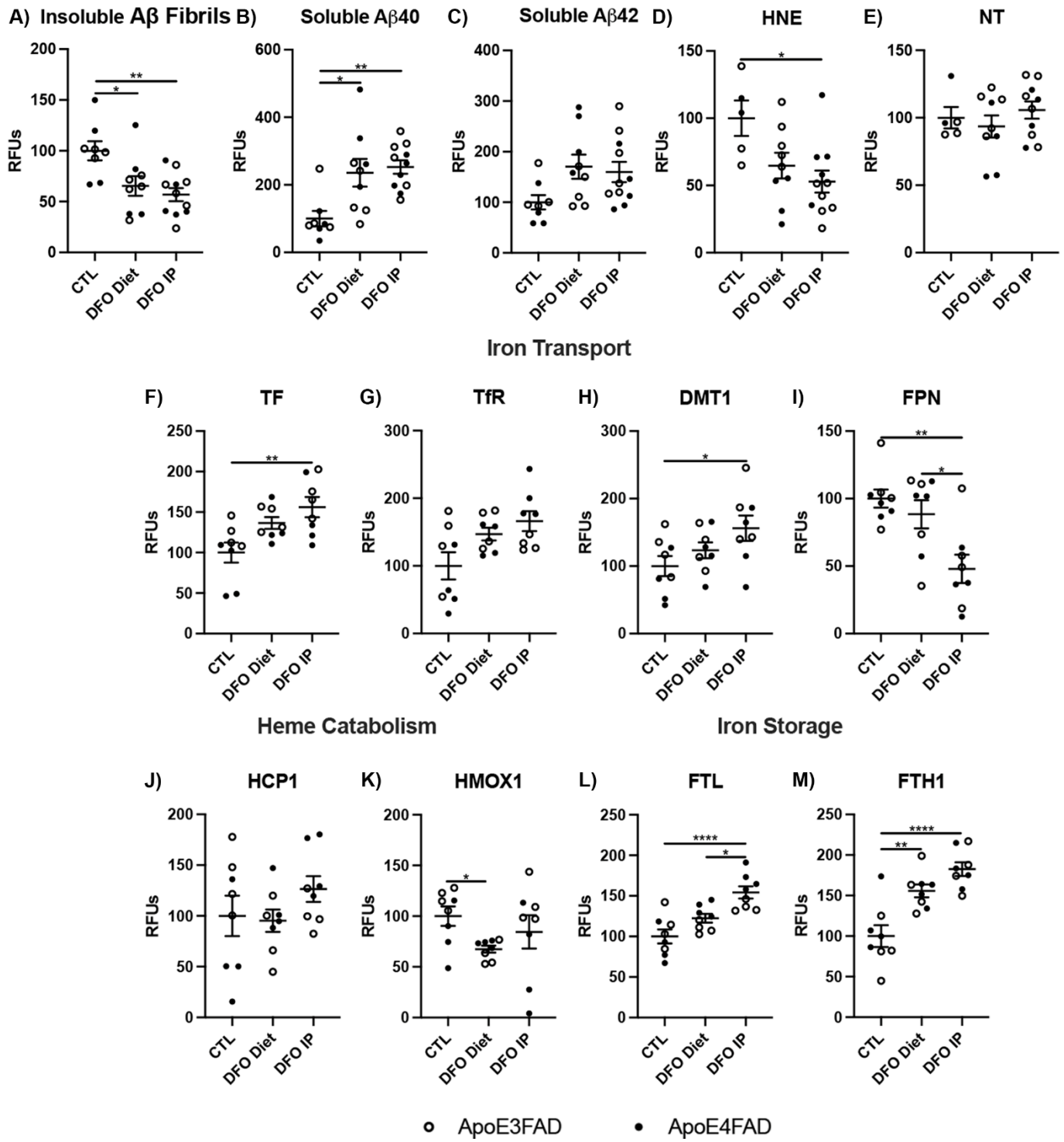

Extended Data Figure 5: DFO chelation of EFAD mouse cortex comparing diet and IP: **A)** insoluble Aβ fibrils, **B)** soluble Aβ40, **C)** soluble Aβ42, **D)** HNE, **E)** NT, **F)** TF, **G)** TfR, **H)** DMT1, **I)** FPN, **J)** HCP1, **K)** HMOX1, **L)** FTL, and **M)** FTH1. Significance, 2-tailed t-test: *p<0.05, **p<0.01, ***p<0.001, ****p<0.0001.

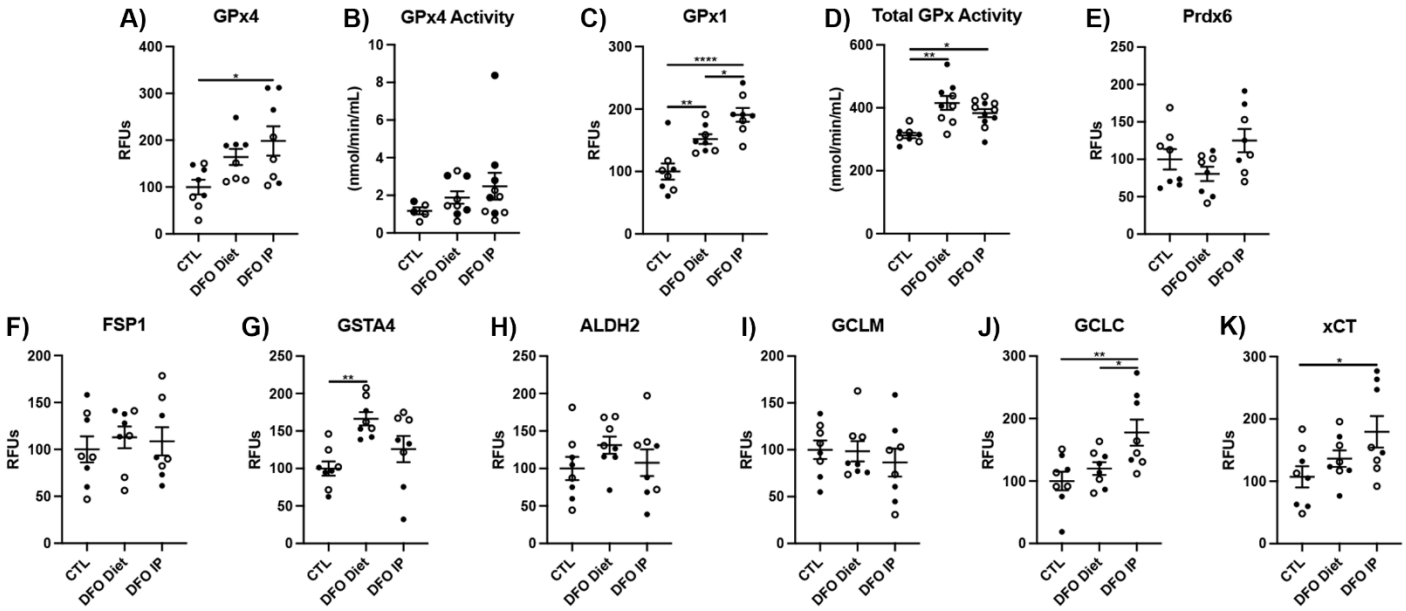

Extended Data Figure 6: DFO chelation of EFAD mouse cortex comparing diet and IP: **A)** GPx4, **B)** GPx4 activity, **C)** GPx1, **D)** GPx1 activity, **E)** Prdx6, **F)** FSP1, **G)** GSTA4, **H)** ALDH2, **I)** GCLM, **J)** GCLC, **K)** xCT. Significance, one-way ANOVA with Tukey's posthoc test (A-K): *p<0.05, **p<0.01, ***p<0.001, ****p<0.0001.

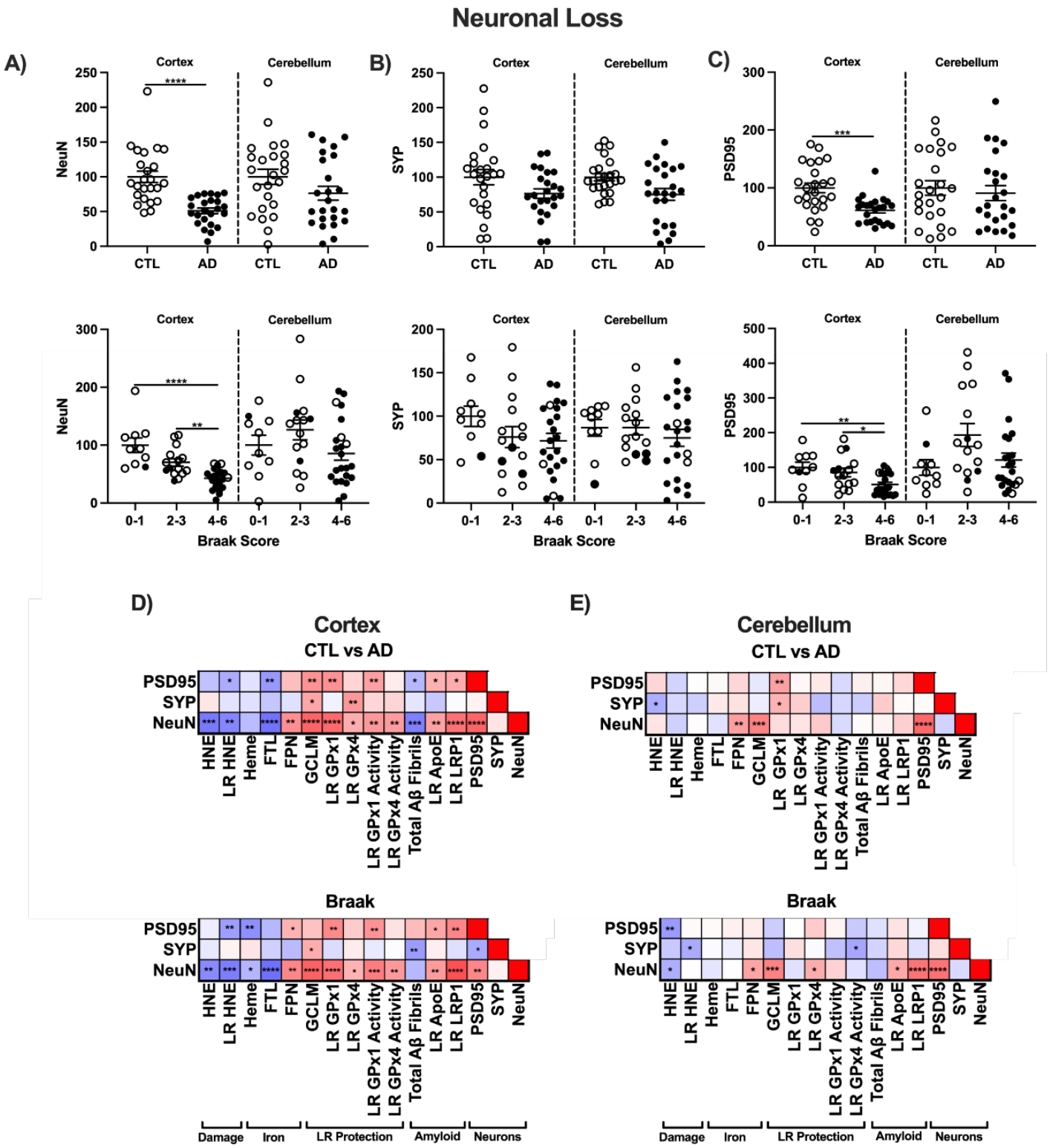

Extended Figure 7: Neuronal loss in AD. Western blots as relative fluorescent units (RFUs) of neuronal markers shown by clinical CTL vs AD or Braak stage[41]. **A)** neuronal nuclei antigen (NeuN), **B)** synaptophysin 1 (SYP), **C)** postsynaptic density protein 95 (PSD95). Correlation matrixes for variables with significant relationships to NeuN for **D)** prefrontal cortex and **E)** cerebellum. Significance by 2- tailed t-test (CTL vs AD), One-way ANOVA (Braak) with Tukey's posthoc, or by Spearman correlation: *p<0.05, **p<0.01, ***p<0.001, ****p<0.0001.

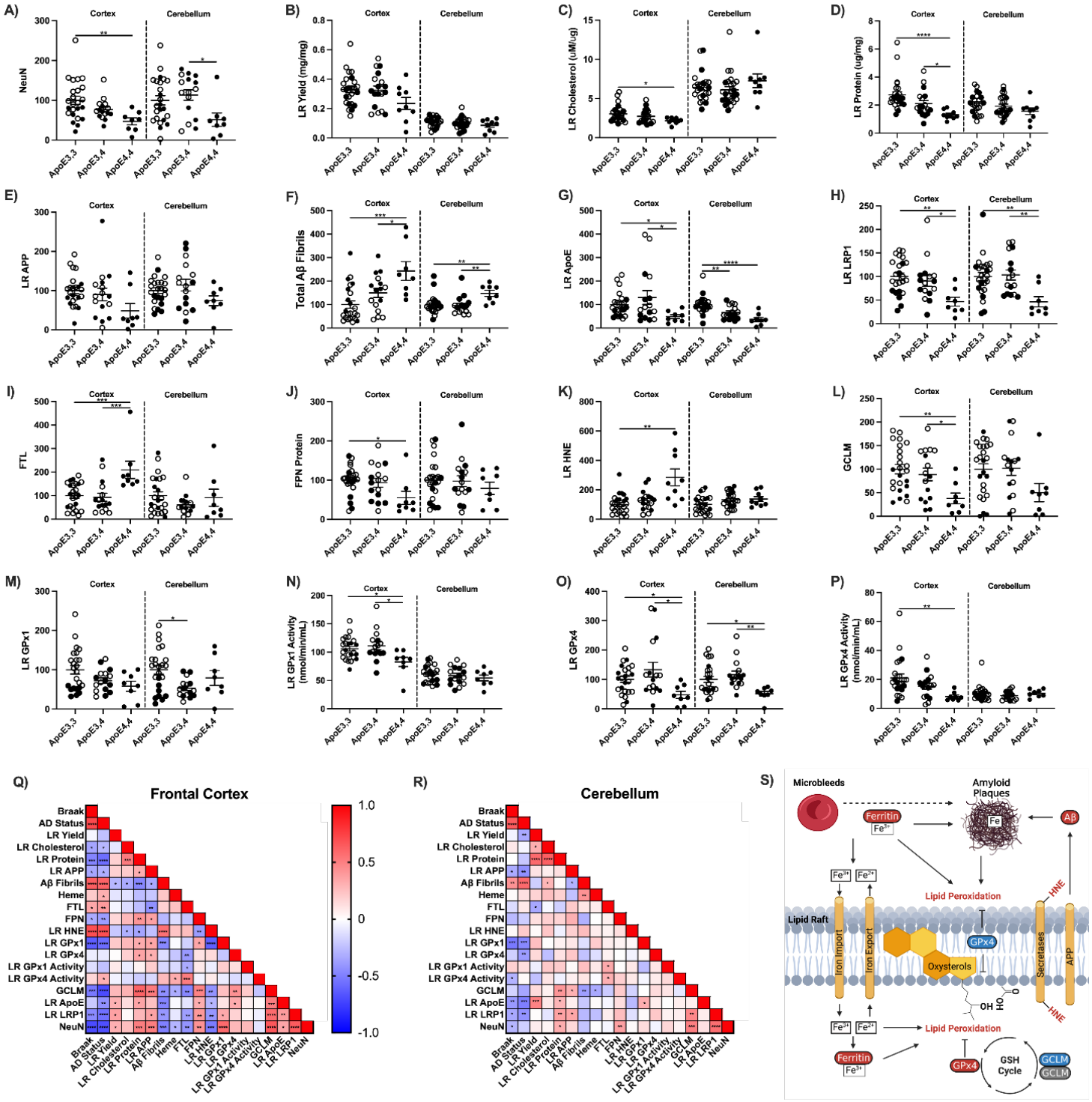

Extended Figure 8: ApoE allele differences in lipid rafts, antioxidant defense, and amyloid. Levels of **A)** NeuN, **B)** LR yield, **C)** LR cholesterol, **D)** total LR protein, **E)** LR APP, **F)** total Aβ fibrils, **G)** LR ApoE, **H)** LR LRP1, **I)** FTL, **J)** FPN, **K)** LR HNE, **L)** GCLM, **M)** LR GPx1, **N)** LR GPx1 activity, **O)** LR GPx4, and **P)** LR GPx4 activity in prefrontal cortex and cerebellum of cognitively normal (open circles) and demented (closed circles). Correlation matrix of proteins analyzed by ApoE allele in **Q)** frontal cortex and **R)** cerebellum. **S)** Schematic hypothesis linking oxidized lipid rafts to amyloid processing. One way ANOVA with Tukey's posthoc, or by Spearman correlation: *p<0.05, **p<0.01, ***p<0.001, ****p<0.0001.

654 **DISCUSSION:**

655 Iron is increasingly implicated in brain oxidative damage during AD[21,46,47]. We report the most
656 comprehensive assessment of iron and its associated proteins in postmortem human aging brain.
657 These new data strongly associate iron with antioxidant defenses and lipid peroxidation that vary by
658 brain region for oxidative damage during AD. We introduce an approach to minimize confounds from
659 vascular and entrapped blood by gentle washing that is validated in mouse brain. This increase in
660 oxidative damage of lipids is associated with altered antioxidant defense pathways. Detailed
661 examination of membrane subfractions showed changes specific to lipid rafts where amyloid is
662 processed. ApoE4 allele carriers had increased oxidative damage with AD. The hypothesized role of
663 iron was tested in a mouse model with the iron chelator DFO. In EFAD mice 1-week of DFO
664 treatment solubilized fibrillar amyloid, consistent with the role of iron in amyloid plaques. This release
665 of entrapped iron on amyloid fibrils is relevant to ongoing clinical trials in which monoclonal therapies
666 dissolve amyloid plaques which must release iron.

667 Heme levels were elevated in AD brains after exogenous blood was minimized. The residual
668 heme may come from leakage from the BBB or microbleeds[48,49]. Heme iron is liberated by heme
669 oxygenase and stored after conversion of ferrous iron to ferric by ferroxidase in FTH1[50] and then
670 packaged on FTL. Since FTL increased with AD, this is indicative of excess iron in AD despite not
671 observing differences in tissue iron. Plaques and NFTs also contain ferritin protein and iron[46,51–53] and
672 iron also directly influences amyloid peptide production by the iron-response element in the APP
673 primary transcript[54]. Reexamination of data from Good et al 1992 shows neighboring CA1 neurons
674 without NFTs had 50% less cytoplasmic iron (**Table S2**)[45]. Additionally, ferroportin which is the sole
675 iron export protein was decreased in both brain regions with AD. Lowered FPN exacerbates
676 ferroptosis in neuroblastoma cells treated with erastin[55]. Altogether, these data are consistent with the
677 ferroptotic hypothesis that excess iron is a mechanism in AD pathogenesis.

678 In addition to changes in iron and iron-related pathways, a loss of detoxification pathways and an
679 increase in oxidative damage contributes to AD pathology. Lipid peroxidation can cause production of
680 reactive alpha-beta unsaturated aldehydes with HNE being the most common. Free HNE is cleared
681 through glutathione s-transferase family members, primarily GSTA4 in the brain, or ALDH2, which is
682 GSH-independent. GSH is needed for most of these processes which has been reported depleted
683 during AD[56,57], likely from the low levels of GCLM shown in these data. GCLM increases the rate of
684 catalysis over 4-fold for production of γ-glutamylcysteine and is the rate-limiting step in GSH
685 biosynthesis[39]. Cysteine availability is also rate-limiting from its primary source, cystine, which is
686 imported by xCT. Independent of GSH, lipid peroxidation is also attenuated by ferroptosis suppressor
687 protein 1 (FSP1) via the quinol cycle[58], which we showed is decreased in AD prefrontal cortex and
688 cerebellum. GSH and quinol cycles both rely on NAPDH produced from the pentose phosphate
689 pathway from G6PD and PGD. G6PD is rate-limiting in the formation of NAPDH[59] and was also
690 decreased in AD prefrontal cortex. All of these antioxidants and iron metabolic proteins are regulated
691 by transcriptional by Nrf2, which is decreased during AD[60,61], also shown here. Decreases in GCLM,
692 FSP1, and G6PD with AD hinder the antioxidant systems which neutralize lipid peroxidation.

693 We also introduce the lipid raft to oxidative repair mechanisms in AD. Lipid rafts are tightly packed
694 microdomains rich in cholesterol, sphingomyelin, and phosphatidylcholine within cellular
695 membranes[62,63]. Lipid classes within the raft are easily oxidized enzymatically (lipoxygenases) or
696 nonenzymatically, by Fenton chemistry[64]. Altered composition of lipid classes within lipid rafts impairs
697 biochemical signal transduction[65] that can cause cell death[66]. Additionally, sterols are more oxidizable
698 that polyunsaturated fatty acids, contrary to prior reports[67]. Oxidation of lipids within rafts may be
699 responsible for the decreased raft yield we reported for AD[41]. ApoE4 carriers also had the lowest raft
700 cholesterol, which introducing new mechanisms for the E4 allele because low cholesterol levels in
701 lipid rafts disrupts raft signaling that can cell death[68].

702 Membrane lipids are protected by GPx4 and Prdx6, which chemically reduce oxidized
703 phospholipids and sterols with GSH[69,70]. We defined lipid rafts for glutathione peroxidases (GPx1-8)
704 which contained only GPx1 and GPx4 but not Prdx6. Prdx6 and GPx1 also reduce lipid
705 hydroperoxides[70] released from membrane lipids[71] and may therefore play a secondary role in

706 defense against ferroptosis. The absence of Prdx6 in the lipid raft fraction is consistent with its
707 transient interactions with membranes[72,73]. AD rafts had lower GPx4 and GPx1 protein and
708 correspondingly lower enzyme activity, consistent with the prominent lipid peroxidation in AD. The
709 non-raft membrane fraction showed minimal oxidation with AD. Furthermore, baseline GPx4 is 2-fold
710 higher in lipid rafts of normal brains than in the non-raft membrane fraction, suggesting that lipid rafts
711 are hotspots for iron-mediated oxidative damage. The observed increases in whole cell GPx4, but
712 with decreased lipid raft GPx4, suggests a localization issue. Cytosolic GPx4 is 20 kDa, while the
713 mitochondrial isoform of 23 kDa containing a leader sequence cleaved for mitochondrial membrane
714 localization[74]. It is possible leader sequences may be needed for membrane localization. Localization
715 may also be mediated by a phosphorylation site that localizes GPx4 to membranes[75].
716 Because lipid rafts are the main site of amyloid production, their lipid peroxidation may alter APP
717 processing enzymes. APP processing is enhanced by the γ-secretase in rat cortex neurons and
718 human neuronal cells exposed to 1-10 μM HNE or 100 μM $FeSO_4$[76]. Moreover, H_2O_2 increased
719 BACE1 activity, the primary secretase responsible for amyloid peptide production in mouse neuronal
720 N2a cells transgenic for human APP_{695}[77]. HNE adducts can impact enzyme activities including
721 GCLM, Prdx6, G6PD, among others relevant to antioxidant defense[78]. APP processing enzymes
722 contain at least 10% of the amino acids His, Lys, Arg, and Tyr that can be covalently linked by HNE
723 or nitrotyrosine. BACE1 (57/501), PSEN1 (50/467), ADAM10 (142/748). BACE1 activity also
724 increases with AD in prefrontal cortex[79] and serum[80,81] paralleling the increases of lipid peroxidation in
725 serum and tissue[82,83]. Future studies will evaluate how lipid raft oxidation alters APP processing for
726 amyloid peptides.
727 AD also decreased Nrf2, a transcriptional regulator of gene responses for oxidative repair that
728 include glutathione peroxidases and GSH biosynthesis proteins[84,85]. Besides our data showing Nrf2
729 levels decline by 75% in the AD cortex but not cerebellum, previous work from coauthors showed
730 decline of Nrf2 mediated antioxidant defenses in aging mouse cerebellum[86,87]. We suggest that the
731 age-related decline of Nrf2 defense enhances membrane oxidation that may increase amyloid
732 peptide production from microbleed iron. There were few changes in iron-related pathways, despite
733 decreased expression of Nrf2 related genes. However, CD163, the hemoglobin-haptoglobin
734 scavenger which increases in response to microbleeds, was shared between brain regions with AD
735 and was among the top responding mRNAs[44]. CD163 is found in microglia[88], which have high levels
736 of ferritin in AD that may arise from microbleeds[53,89,90]. Endogenous cell ferritin merits consideration
737 because microglia and astrocytes in young rat brain have 2-fold more ferritin than neurons, while
738 oligodendroglia have the highest ferritin levels[91].
739 New AD changes are shown for multiple transcription factors. While Nrf2 is greatly lowered in AD
740 (see above), there are major increases of NF-kB and NCOA4. NF-kB regulates several pro-oxidant
741 enzymes while NCOA4 responds to iron excess for by lysosomal degradation iron bound proteins
742 (ferritinophagy)[43]. A relationship of NF-kB to membrane oxidation is suggested by its role in
743 ferroptosis of glioblastoma cells treated with a GPx4 inhibitor[92]. Future studies will supersede this bulk
744 analysis which cannot resolve cell type specificity for iron-mediated damage.
745 Finally, ApoE4,4 carriers had the greatest oxidative damage in AD brains and lowest antioxidant
746 protection in lipid rafts, which contrasts with an *in vitro* study of rat neurons with human ApoE
747 alleles[93]. ApoE alleles may also differentially alter antioxidant gene regulation in brain consistent with
748 their roles in Aβ clearance and inflammation[94]. Our findings introduce the ApoE alleles as important to
749 iron-mediated processes for further discussion of ferroptosis.
750 Lastly, we experimentally tested the role of iron with acute deferoxamine (DFO) in EFAD mice.
751 Chelation therapy for AD was first attempted in 1991 to remove aluminum by DFO, which slowed
752 cognitive decline during 24-months[95]. While the cognitive benefits of DFO were attributed to
753 aluminum chelation, Gleason and Bush[96] also noted that DFO has 6-fold greater affinity for ferric iron
754 than aluminum. Our DFO data directly supports the major role of iron in multiple AD pathologies, as
755 DFO reduced HNE oxidation and decreased amyloid fibrils. This suggests that iron chelation may
756 solubilize amyloid fibrils to monomers while liberating iron. Traumatic brain injury, which often results
757 in microbleeds, shows increases in amyloid levels that are attenuated with DFO treatment[97]. We

758 previously showed that microbleeds precede amyloid formation and that these two pathologies
759 colocalize in the EFAD mice[98]. Is it possible that amyloid production has a role in preventing more
760 heme-derived iron from entering and depositing in the brain parenchyma? Furthermore, if iron is
761 liberated from amyloid fibrils, then oxidative damage would be expected in the absence of chelation.
762 DFO treatment increased Nrf2 and downstream antioxidants together with decreased oxidative
763 damage, that support DFO clinical value. Current amyloid monoclonal therapies that target
764 aggregated amyloid must also liberate labile iron. The liberated iron could contribute to amyloid
765 related imaging abnormalities (ARIA) of clinical trials[99–101]. Combination therapies should be
766 considered for iron chelators with amyloid monoclonal treatment.
767 In summary, this analysis of iron metabolism and membrane oxidation in AD is the first to
768 comprehensively document the network of proteins that mediate iron transport and GSH-mediated
769 neuroprotection relevant to ferroptosis. AD pathway specificity was demonstrated by the greater
770 changes in the prefrontal cortex than cerebellum, consistent with quantitative differences in their AD
771 neuropathology. Our data identify novel alterations in iron related transport, clearance, and oxidative
772 repair mechanisms in relation to lipid rafts and APP processing. Moreover, multiple anti-ferroptotic
773 pathways are implicated by the decreases in GCLM, FSP1, FPN, and lipid raft GPx4. Experimental
774 reduction of lipid peroxidation by iron chelation may be considered for co-therapy with monoclonal
775 antibody treatments to reduce amyloid that inevitably releases iron associated with amyloid plaques.
776 Taken together, this suite of findings confirms that iron can contribute to AD pathology by
777 exacerbating oxidative damage.
778
779 **METHODS:**
780 Human Samples Postmortem prefrontal cortex and cerebellum with Braak scores were provided by
781 three Alzheimer's Disease Centers: University of Southern California (Dr. Carol Miller), University of
782 California Irvine (UCI MIND), and University of Washington (BRaIN). Samples were genotyped for
783 ApoE alleles by PCR for SNP variants rs429358 and rs7412. All human subjects provided informed
784 consent. Human tissue use was approved through IRB protocol #UP-20-00014-EXEMPT. Details for
785 individual brains are in **Supplementary Table 1**.
786
787 Mice C57BL/6 mice from Jackson laboratories or ApoEFAD mice from Mary Jo LaDu (University of
788 Illinois, Chicago) were housed by the University of Southern California's Department of Animal
789 Resources. Mice had ad libitum access to Purina Lab Chow (LabDiet, Hayward, CA) and water. Mice
790 were housed in groups of 5 at 22°C/ 30% humidity, with standard nesting material and light cycles of
791 0600-1800 hr. Studies were approved by the USC Animal Use and Care Committee (IACUC# 20417).
792 Female ApoEFAD mice were given DFO treatment either in rodent chow (10mg/kg/day) for two
793 weeks or by intraperitoneal injection twice daily for one week (10m/kg/day). At 6-months old mice
794 were anesthetized with isoflurane and euthanized by cardiac puncture. C57BL/6 mouse cortex was
795 collected as non-perfused, with transcardial PBS perfusion, or PBS perfusion + 10U/mL heparin
796 (Sigma-Aldrich, St. Louis, MO). Tissues were stored at -80°C.
797
798 Tissue Washing Human and mouse brain tissue was thawed on ice and minced by ceramic scalpel
799 for iron and heme measurements or by surgical scissors. PBS (10 volumes) was placed in each tube
800 and the samples were gently washed by two cycles of vortexing and collected by gentle centrifugation
801 800g/30 sec/4°C. PBS was retained on a small subset of samples and further spun at 4,000g/10 min/
802 4°C. The pellet was sonicated 10 sec at 50% power in PBS. Resuspended pellet and lysate were
803 assayed for heme (**Table 1; Fig. S1**).
804
805 Amyloid Measurements Human tissue was processed for amyloid measurements as previously
806 described[41]. Briefly, tissue was homogenized in RIPA without SDS and spun for 10,000g for 1h at
807 4°C. Supernatant was collected and analyzed for soluble Aβ fibrils using M78 (Conformation specific
808 antibody for Aβ fibrils[102], a gift from Dr. Charles Glabe, UCI). The residual pellet was resuspended in
809 70% formic acid and sonicated. The resuspension was nutated at room temperature for 2h and

810 neutralized with 20 volumes of 1M Tris and concentrated with a vacuum concentrator (Labconco,
811 Kansas City, MO). Amyloid levels were assayed by dot blot and visualized as described below for
812 Western blots.
813
814 Lipid Raft and Non-Raft Membrane The lipid raft fraction was isolated from 40 mg tissue
815 homogenates of frozen prefrontal cortex (Brodmann area 8, 9 or 10) and cerebellum using a column-
816 based isolation kit (Invent Biotechnologies, Plymouth, MN). These findings were verified by sucrose
817 gradient ultracentrifugation[103]. Lipid raft and the remaining detergent soluble non-raft membrane
818 (NRM) fractions were resuspended in PBS+1% triton x-100 and sonicated 10 seconds at 50% power.
819 Protein was assayed by the copper-based 660 nm assay (ThermoFisher Scientific, Waltham, MA).
820 Lipid raft enrichment and purity were determined by cytosolic GAPDH, several lipid raft markers
821 including flotillin1, and nuclear marker H3[41].
822
823 Nuclear Isolation 20 mg of frozen brain was homogenized in 125uL of sucrose buffer for nuclear and
824 cytosolic fractions. A previously published protocol[104] was modified for brain tissue by adding 1% NP-
825 40 to the first wash step, resuspending the pellet, and incubating on ice for 30 min. Nuclear and
826 cytosolic extractions were cross probed for purity against both H3 and GAPDH by Western blot[105] and
827 showed the expected enrichment (**Fig. S5**).
828
829 Western Blot Proteins from lipid rafts (5 ug), whole cell lysate (20 ug), or nuclear fractions (20 ug)
830 were heated at 75°C under denaturing conditions and resolved on 4-20% gradient gels. Proteins were
831 electroblotted using a Criterion blotter (Bio-Rad Laboratories, Hercules, CA) and transferred onto
832 0.45um polyvinyl difluoride membranes. Membranes were stained using Revert 700 fluorescent
833 protein stain and imaged prior to blocking with LI-COR Intercept blocking buffer (LI-COR Biosciences,
834 Lincoln, NE), followed by primary antibodies. Membranes were incubated with IRDye 800CW and/or
835 700CW secondary antibodies and visualized by Odyssey (LI-COR Biosciences). Western blot data
836 was quantified with ImageJ and normalized by total protein per lane and/or loading control protein.
837
838 Biochemical Assays Lipid rafts were assayed for total cholesterol (Cell Biolabs, San Diego, CA).
839 Tissue hemoglobin or heme quantified by Quantichrom assay (BioAssay Systems, Hayward, CA). α-
840 Hemoglobin was quantified by ELISA (ThermoFisher Scientific, Waltham, MA). Total glutathione
841 peroxidase activities were measured by enzymatic assay (Cayman Chemical, Ann Arbor, MI). GPx4
842 activity was assayed by generating oxidized phosphatidylcholine using soybean lipoxygenase[106].
843 Purified PCOOH was used in place of cumene hydroperoxide in Cayman's total GPx activity assay at
844 a concentration of 30μM per well.
845
846 ICP-MS 50mg of brain tissue was cut with a ceramic scalpel and placed in metal free certified test
847 tubes. Tissues were washed twice with PBS and homogenized in PBS by polyethylene pestle (PES-
848 15-B-SI, Axygen) with purified water (18.2 MΩ; Millipore, Burlington, MA) treated with Chelex 100
849 (sigma, St. Louis, MO). Homogenates were desiccated by vacuum centrifuge at 95°C for 90 min. and
850 solubilized in trace metal free 70% HNO_3 overnight. 30% H_2O_2 was then added followed by
851 dessication. After resuspension in 2% HNO_3, samples were analyzed by Agilent 7500ce ICP-MS in
852 hydrogen mode with a practical detection limit of 10ppb and a relative standard deviation (RSD) of
853 replicate measures between 0.2 to 5%. Total iron concentration was normalized to wet weight tissue.
854
855 RNA-Sequencing 20mg of brain tissue was homogenized in TRIzol reagent using a BeadBug
856 Benchtop Homogenizer. Brain tissue was suspended in 1 mL of TRIzol and homogenized for 6
857 rounds of 10 s homogenization and 60 s holds between each round. 300 μL of chloroform was added
858 to the sample and aqueous separation of RNA was performed using centrifugation in a heavy gel
859 phase-lock tube (VWR, 10847-802). The aqueous phase was applied to a standard column-based
860 RNA purification kit (Quantabio, Extracta Plus, Cat# 95214-050) following the manufacturer's
861 protocol. Library preparation and RNA sequencing was performed by Novogene. Reads from

samples with were processed using trim_galore (0.6.5-1) and mapped to the GRCh38.p14 genome with STAR-2.7.10a. Mapped reads were counted to genes using featureCounts (Subread-2.0.3) and the GRCh38.108 GTF file. Unwanted noise and artifacts were removed using svaseq and removeBatchEffects from the sva package-3.42.0 and differential expression analysis was performed with DESeq2-1.34.0 using R-4.3.2. Raw RNA-seq data is available through Annotare: E-MTAB-14167.

Statistics GraphPad Prism 9 software (GraphPad, San Diego, CA) was used for graphing and statistical analysis. Several measures were adjusted by age and sex by multiple linear regression which yielded no significant interactions. For these reasons data were analyzed by two-tailed t-test or one-way ANOVA with Tukey's HSD ($p<0.05$) with a confidence interval set at 95%. Data that were not normally distributed were analyzed by Mann Whitney U or Kruskal-Wallis with Dunn's test. All correlation matrixes used Spearman's correlation for non-linear data.

Acknowledgements & Funding
The authors are grateful to Liying Zhao for performing ICP-MS measurements, and Carol Church and Kymry Jones for assistance with postmortem tissues. The authors appreciate the helpful discussions of brain samples with Carol Miller (USC) and C. Dirk Keene (UW). Tissue for this study was obtained from the USC ADRC Neuropathology Core, NIAAG066530. The UCI-ADRC is funded by NIH/NIA Grant P30AG066519. J. Silva and E. Head were supported by P30AG066519. Lab studies were supported by NIH grants to CEF (R01-AG051521, P50-AG05142, P01-AG055367) and Cure Alzheimer's Fund; Larry L. Hillblom Foundation Grant 2022-A-010-SUP, the Glenn Foundation for Medical Research and AFAR Grant for Junior Faculty Award, and Navigage Foundation Award to RHS; T32AG052374 to GG; and T32-AG000037 (PI: Eileen Crimmins) to MAT. Brain specimens were obtained from ADRC Tissue Cores: USC (P50-AG005142, AG066530); University of California Irvine (P30-AG066519); UW (P30-AG066509; U01-AG006781). Venn diagrams were made with Venny 2.1.0 and schematics made using BioRender.

Ethics Declarations
The authors declare no competing interests.

Data Availability
The authors declare that the data supporting the findings of this study are available within the paper and its supplementary information files. Should any raw data files be needed in another format they are available from the corresponding author upon reasonable request.

References
1. Boyle, P. A. *et al.* To what degree is late life cognitive decline driven by age-related neuropathologies? *Brain* **144**, 2166–2175 (2021).

2. Robinson, J. L. *et al.* The development and convergence of co-pathologies in Alzheimer's disease. *Brain* **144**, 953–962 (2021).

3. Shih, A. Y. *et al.* Cystine/Glutamate Exchange Modulates Glutathione Supply for Neuroprotection from Oxidative Stress and Cell Proliferation. *J. Neurosci.* **26**, 10514–10523 (2006).

4. Yang, W. S. *et al.* Regulation of Ferroptotic Cancer Cell Death by GPX4. *Cell* **156**, 317–331 (2014).

906 5. F, U., M, M., M, V., L, F. & C, G. Purification from pig liver of a protein which protects liposomes
907 and biomembranes from peroxidative degradation and exhibits glutathione peroxidase activity on
908 phosphatidylcholine hydroperoxides. *Biochimica et biophysica acta* **710**, (1982).
909 6. Cozza, G. *et al.* Glutathione peroxidase 4-catalyzed reduction of lipid hydroperoxides in
910 membranes: The polar head of membrane phospholipids binds the enzyme and addresses the
911 fatty acid hydroperoxide group toward the redox center. *Free Radical Biology and Medicine* **112**,
912 1–11 (2017).
913 7. Torres-Velarde, J. M. *et al.* Peroxiredoxin 6 suppresses ferroptosis in lung endothelial cells. *Free*
914 *Radical Biology and Medicine* (2024) doi:10.1016/j.freeradbiomed.2024.04.208.
915 8. Wang, S., Wang, H., Zhu, S. & Li, F. Systematical analysis of ferroptosis regulators and
916 identification of GCLM as a tumor promotor and immunological biomarker in bladder cancer.
917 *Front. Oncol.* **12**, (2022).
918 9. Stockwell, B. R. Ferroptosis turns 10: Emerging Mechanisms, Physiological Functions, and
919 Therapeutic Applications. *Cell* **185**, 2401–2421 (2022).
920 10. Goodman, L. Alzheimer's disease; a clinico-pathologic analysis of twenty-three cases with a
921 theory on pathogenesis. *J Nerv Ment Dis* **118**, 97–130 (1953).
922 11. Yang, S.-S. *et al.* High Morphologic Plasticity of Microglia/Macrophages Following Experimental
923 Intracerebral Hemorrhage in Rats. *International Journal of Molecular Sciences* **17**, 1181 (2016).
924 12. Lovell, M. A., Ehmann, W. D., Mattson, M. P. & Markesbery, W. R. Elevated 4-hydroxynonenal in
925 ventricular fluid in Alzheimer's disease. *Neurobiol Aging* **18**, 457–461 (1997).
926 13. Markesbery, W. R. & Lovell, M. A. Four-hydroxynonenal, a product of lipid peroxidation, is
927 increased in the brain in Alzheimer's disease. *Neurobiol Aging* **19**, 33–36 (1998).
928 14. Dixon, S. J. *et al.* Ferroptosis: an iron-dependent form of nonapoptotic cell death. *Cell* **149**, 1060–
929 1072 (2012).
930 15. Ma, H., Dong, Y., Chu, Y., Guo, Y. & Li, L. The mechanisms of ferroptosis and its role in
931 alzheimer's disease. *Front. Mol. Biosci.* **9**, (2022).

932 16. Jakaria, M., Belaidi, A. A., Bush, A. I. & Ayton, S. Ferroptosis as a mechanism of
933 neurodegeneration in Alzheimer's disease. *J Neurochem* **159**, 804–825 (2021).
934 17. Wang, Q. *et al.* Ferroptosis, Pyroptosis, and Cuproptosis in Alzheimer's Disease. *ACS Chem.*
935 *Neurosci.* **14**, 3564–3587 (2023).
936 18. Ashraf, A., Jeandriens, J., Parkes, H. G. & So, P.-W. Iron dyshomeostasis, lipid peroxidation and
937 perturbed expression of cystine/glutamate antiporter in Alzheimer's disease: Evidence of
938 ferroptosis. *Redox Biol* **32**, 101494 (2020).
939 19. Raha, A. A. *et al.* Interplay of Ferritin Accumulation and Ferroportin Loss in Ageing Brain:
940 Implication for Protein Aggregation in Down Syndrome Dementia, Alzheimer's, and Parkinson's
941 Diseases. *Int J Mol Sci* **23**, 1060 (2022).
942 20. Bao, W.-D. *et al.* Loss of ferroportin induces memory impairment by promoting ferroptosis in
943 Alzheimer's disease. *Cell Death Differ* **28**, 1548–1562 (2021).
944 21. Ayton, S. *et al.* Regional brain iron associated with deterioration in Alzheimer's disease: A large
945 cohort study and theoretical significance. *Alzheimer's & Dementia* **17**, 1244–1256 (2021).
946 22. Hambright, W. S., Fonseca, R. S., Chen, L., Na, R. & Ran, Q. Ablation of ferroptosis regulator
947 glutathione peroxidase 4 in forebrain neurons promotes cognitive impairment and
948 neurodegeneration. *Redox Biology* **12**, 8–17 (2017).
949 23. Balusu, S. *et al.* MEG3 activates necroptosis in human neuron xenografts modeling Alzheimer's
950 disease. *Science* **381**, 1176–1182 (2023).
951 24. Müller, T. *et al.* Necroptosis and ferroptosis are alternative cell death pathways that operate in
952 acute kidney failure. *Cell Mol Life Sci* **74**, 3631–3645 (2017).
953 25. Wood, P. L. The Cerebellum in AD. in *Neuroinflammation: Mechanisms and Management* (ed.
954 Wood, P. L.) 295–300 (Humana Press, Totowa, NJ, 2003). doi:10.1007/978-1-59259-297-5_15.
955 26. Farr, A. C. & Xiong, M. P. Challenges and Opportunities of Deferoxamine Delivery for Treatment
956 of Alzheimer's Disease, Parkinson's Disease, and Intracerebral Hemorrhage. *Mol Pharm* **18**, 593–
957 609 (2021).

958 27. Ayton, S. *et al.* Brain iron is associated with accelerated cognitive decline in people with Alzheimer
959 pathology. *Mol Psychiatry* **25**, 2932–2941 (2020).
960 28. LeVine, S. M., Wulser, M. J. & Lynch, S. G. Iron quantification in cerebrospinal fluid. *Anal*
961 *Biochem* **265**, 74–78 (1998).
962 29. Erikson, K. M., Pinero, D. J., Connor, J. R. & Beard, J. L. Regional brain iron, ferritin and
963 transferrin concentrations during iron deficiency and iron repletion in developing rats. *J Nutr* **127**,
964 2030–2038 (1997).
965 30. Ayton, S., Faux, N. G., Bush, A. I., & Alzheimer's Disease Neuroimaging Initiative. Ferritin levels
966 in the cerebrospinal fluid predict Alzheimer's disease outcomes and are regulated by APOE. *Nat*
967 *Commun* **6**, 6760 (2015).
968 31. Petzold, A. *et al.* Cerebrospinal fluid ferritin levels, a sensitive diagnostic test in delayed
969 presenting subarachnoid haemorrhage. *J Stroke Cerebrovasc Dis* **20**, 489–493 (2011).
970 32. Cazzola, M. *et al.* Biologic and clinical significance of red cell ferritin. *Blood* **62**, 1078–1087 (1983).
971 33. McIlwain, H. & Bachelard, H. S. *Biochemistry and the Central Nervous System*. (Churchill
972 Livingstone, Edinburgh, 1985).
973 34. Montine, T. J. *et al.* Lipid peroxidation in aging brain and Alzheimer's disease. *Free Radic Biol*
974 *Med* **33**, 620–626 (2002).
975 35. Zhu, D., Montagne, A. & Zhao, Z. Alzheimer's pathogenic mechanisms and underlying sex
976 difference. *Cell Mol Life Sci* **78**, 4907–4920 (2021).
977 36. Xie, Z. *et al.* Peroxynitrite Mediates Neurotoxicity of Amyloid β-Peptide1–42- and
978 Lipopolysaccharide-Activated Microglia. *J Neurosci* **22**, 3484–3492 (2002).
979 37. Dufrusine, B. *et al.* Iron-Dependent Trafficking of 5-Lipoxygenase and Impact on Human
980 Macrophage Activation. *Front Immunol* **10**, 1347 (2019).
981 38. Sharma, G. *et al.* Glutathione peroxidase-1 and neuromodulation: Novel potentials of an old
982 enzyme. *Food and Chemical Toxicology* **148**, 111945 (2021).

983 39. Chen, Y., Shertzer, H. G., Schneider, S. N., Nebert, D. W. & Dalton, T. P. Glutamate cysteine
984 ligase catalysis: dependence on ATP and modifier subunit for regulation of tissue glutathione
985 levels. *J Biol Chem* **280**, 33766–33774 (2005).
986 40. Giustarini, D. *et al.* Pitfalls in the analysis of the physiological antioxidant glutathione (GSH) and
987 its disulfide (GSSG) in biological samples: An elephant in the room. *J Chromatogr B Analyt*
988 *Technol Biomed Life Sci* **1019**, 21–28 (2016).
989 41. Thorwald, M. A., Silva, J., Head, E. & Finch, C. E. Amyloid futures in the expanding pathology of
990 brain aging and dementia. *Alzheimers Dement* (2022) doi:10.1002/alz.12896.
991 42. Keberle, H. THE BIOCHEMISTRY OF DESFERRIOXAMINE AND ITS RELATION TO IRON
992 METABOLISM. *Ann N Y Acad Sci* **119**, 758–768 (1964).
993 43. Mancias, J. D., Wang, X., Gygi, S. P., Harper, J. W. & Kimmelman, A. C. Quantitative proteomics
994 identifies NCOA4 as the cargo receptor mediating ferritinophagy. *Nature* **509**, 105–109 (2014).
995 44. Roy-O'Reilly, M. *et al.* Soluble CD163 in intracerebral hemorrhage: biomarker for perihematomal
996 edema. *Ann Clin Transl Neurol* **4**, 793–800 (2017).
997 45. Good, P. F., Perl, D. P., Bierer, L. M. & Schmeidler, J. Selective accumulation of aluminum and
998 iron in the neurofibrillary tangles of Alzheimer's disease: a laser microprobe (LAMMA) study. *Ann*
999 *Neurol* **31**, 286–292 (1992).
000 46. Everett, J. *et al.* Biogenic metallic elements in the human brain? *Sci Adv* **7**, eabf6707 (2021).
001 47. Zeng, Y., DiGiacomo, P. S., Madsen, S. J., Zeineh, M. M. & Sinclair, R. Exploring valence states
002 of abnormal mineral deposits in biological tissues using correlative microscopy and spectroscopy
003 techniques: A case study on ferritin and iron deposits from Alzheimer's disease patients.
004 *Ultramicroscopy* **231**, 113254 (2021).
005 48. Montagne, A. *et al.* Blood-brain barrier breakdown in the aging human hippocampus. *Neuron* **85**,
006 296–302 (2015).

007 49. Bennett, D. A., Schneider, J. A., Bienias, J. L., Evans, D. A. & Wilson, R. S. Mild cognitive
008 impairment is related to Alzheimer disease pathology and cerebral infarctions. *Neurology* **64**,
009 834–841 (2005).
010 50. Arosio, P. & Levi, S. Ferritin, iron homeostasis, and oxidative damage1, 2 1Guest Editor: Mario
011 Comporti 2This article is part of a series of reviews on “Iron and Cellular Redox Status.” The full
012 list of papers may be found on the homepage of the journal. *Free Radical Biology and Medicine*
013 **33**, 457–463 (2002).
014 51. Collingwood, J. F. *et al.* Three-dimensional tomographic imaging and characterization of iron
015 compounds within Alzheimer’s plaque core material. *J Alzheimers Dis* **14**, 235–245 (2008).
016 52. van Duijn, S., Nabuurs, R. J. A., van Duinen, S. G. & Natté, R. Comparison of Histological
017 Techniques to Visualize Iron in Paraffin-embedded Brain Tissue of Patients with Alzheimer’s
018 Disease. *J Histochem Cytochem* **61**, 785–792 (2013).
019 53. Streit, W. J. *et al.* Droplet Degeneration of Hippocampal and Cortical Neurons Signifies the
020 Beginning of Neuritic Plaque Formation. *J Alzheimers Dis* **85**, 1701–1720 (2022).
021 54. Rogers, J. T. *et al.* An iron-responsive element type II in the 5’-untranslated region of the
022 Alzheimer’s amyloid precursor protein transcript. *J Biol Chem* **277**, 45518–45528 (2002).
023 55. Geng, N. *et al.* Knockdown of ferroportin accelerates erastin-induced ferroptosis in neuroblastoma
024 cells. *Eur Rev Med Pharmacol Sci* **22**, 3826–3836 (2018).
025 56. Chen, J. J. *et al.* Altered central and blood glutathione in Alzheimer’s disease and mild cognitive
026 impairment: a meta-analysis. *Alzheimers Res Ther* **14**, 23 (2022).
027 57. Mandal, P. K. *et al.* Hippocampal glutathione depletion with enhanced iron level in patients with
028 mild cognitive impairment and Alzheimer’s disease compared with healthy elderly participants.
029 *Brain Commun* **4**, fcac215 (2022).
030 58. Doll, S. *et al.* FSP1 is a glutathione-independent ferroptosis suppressor. *Nature* **575**, 693–698
031 (2019).

032 59. Eggleston, L. V. & Krebs, H. A. Regulation of the pentose phosphate cycle. *Biochem J* **138**, 425–
033 435 (1974).
034 60. Thorwald, M. A. *et al.* Alzheimer's Disease associations of ferritin and glutathione with oxidative
035 damage and neuronal loss. *bioRxiv* 2023.03.28.534324 (2023) doi:10.1101/2023.03.28.534324.
036 61. De Plano, L. M., Calabrese, G., Rizzo, M. G., Oddo, S. & Caccamo, A. The Role of the
037 Transcription Factor Nrf2 in Alzheimer's Disease: Therapeutic Opportunities. *Biomolecules* **13**,
038 549 (2023).
039 62. Sezgin, E., Levental, I., Mayor, S. & Eggeling, C. The mystery of membrane organization:
040 composition, regulation and roles of lipid rafts. *Nat. Rev. Mol. Cell Biol.* **18**, 361–374 (2017).
041 63. Mesa-Herrera, F., Taoro-González, L., Valdés-Baizabal, C., Diaz, M. & Marín, R. Lipid and Lipid
042 Raft Alteration in Aging and Neurodegenerative Diseases: A Window for the Development of New
043 Biomarkers. *Int J Mol Sci* **20**, 3810 (2019).
044 64. Gaschler, M. M. & Stockwell, B. R. Lipid peroxidation in cell death. *Biochem Biophys Res*
045 *Commun* **482**, 419–425 (2017).
046 65. Zhu, Y. *et al.* Lowering glycosphingolipid levels in CD4+ T cells attenuates T cell receptor
047 signaling, cytokine production, and differentiation to the Th17 lineage. *J Biol Chem* **286**, 14787–
048 14794 (2011).
049 66. Park, S.-Y. *et al.* Lipid raft-disrupting miltefosine preferentially induces the death of colorectal
050 cancer stem-like cells. *Clin Transl Med* **11**, e552 (2021).
051 67. Saito, Y., Noguchi, N. & Niki, E. Cholesterol is more readily oxidized than phospholipid linoleates
052 in cell membranes to produce cholesterol hydroperoxides. *Free Radic Biol Med* **211**, 89–95
053 (2024).
054 68. George, K. S. & Wu, S. Lipid Raft: A Floating Island Of Death or Survival. *Toxicol Appl Pharmacol*
055 **259**, 311–319 (2012).

056 69. Thomas, J. P., Geiger, P. G., Maiorino, M., Ursini, F. & Girotti, A. W. Enzymatic reduction of
057 phospholipid and cholesterol hydroperoxides in artificial bilayers and lipoproteins. *Biochimica et*
058 *Biophysica Acta (BBA) - Lipids and Lipid Metabolism* **1045**, 252–260 (1990).
059 70. Fisher, A. B. Peroxiredoxin 6 in the repair of peroxidized cell membranes and cell signaling. *Arch*
060 *Biochem Biophys* **617**, 68–83 (2017).
061 71. Lubos, E., Loscalzo, J. & Handy, D. E. Glutathione Peroxidase-1 in Health and Disease: From
062 Molecular Mechanisms to Therapeutic Opportunities. *Antioxid Redox Signal* **15**, 1957–1997
063 (2011).
064 72. Chatterjee, S. *et al.* Peroxiredoxin 6 phosphorylation and subsequent phospholipase A2 activity
065 are required for agonist-mediated activation of NADPH oxidase in mouse pulmonary
066 microvascular endothelium and alveolar macrophages. *J Biol Chem* **286**, 11696–11706 (2011).
067 73. Vázquez-Medina, J. P. *et al.* Genetic inactivation of the phospholipase A2 activity of peroxiredoxin
068 6 in mice protects against LPS-induced acute lung injury. *Am J Physiol Lung Cell Mol Physiol* **316**,
069 L656–L668 (2019).
070 74. Arai, M. *et al.* Import into mitochondria of phospholipid hydroperoxide glutathione peroxidase
071 requires a leader sequence. *Biochem Biophys Res Commun* **227**, 433–439 (1996).
072 75. Wu, K. *et al.* Creatine kinase B suppresses ferroptosis by phosphorylating GPX4 through a
073 moonlighting function. *Nat Cell Biol* **25**, 714–725 (2023).
074 76. Gwon, A.-R. *et al.* Oxidative lipid modification of nicastrin enhances amyloidogenic γ-secretase
075 activity in Alzheimer's disease. *Aging Cell* **11**, 559–568 (2012).
076 77. Kwak, Y.-D. *et al.* Differential regulation of BACE1 expression by oxidative and nitrosative signals.
077 *Molecular Neurodegeneration* **6**, 17 (2011).
078 78. Milkovic, L., Zarkovic, N., Marusic, Z., Zarkovic, K. & Jaganjac, M. The 4-Hydroxynonenal–Protein
079 Adducts and Their Biological Relevance: Are Some Proteins Preferred Targets? *Antioxidants*
080 *(Basel)* **12**, 856 (2023).

081 79. Fukumoto, H., Cheung, B. S., Hyman, B. T. & Irizarry, M. C. Beta-secretase protein and activity
082 are increased in the neocortex in Alzheimer disease. *Arch Neurol* **59**, 1381–1389 (2002).
083 80. Zuliani, G. *et al.* Increased blood BACE1 activity as a potential common pathogenic factor of
084 vascular dementia and late onset Alzheimer's disease. *Sci Rep* **10**, 14980 (2020).
085 81. Hampel, H. *et al.* The β-Secretase BACE1 in Alzheimer's Disease. *Biological Psychiatry* **89**, 745–
086 756 (2021).
087 82. McGrath, L. T. *et al.* Increased oxidative stress in Alzheimer's disease as assessed with 4-
088 hydroxynonenal but not malondialdehyde. *QJM* **94**, 485–490 (2001).
089 83. Smith, M. A., Harris, P. L. R., Sayre, L. M. & Perry, G. Iron accumulation in Alzheimer disease is a
090 source of redox-generated free radicals. *Proceedings of the National Academy of Sciences* **94**,
091 9866–9868 (1997).
092 84. M, R.-G. *et al.* Sensitivity to carcinogenesis is increased and chemoprotective efficacy of enzyme
093 inducers is lost in nrf2 transcription factor-deficient mice. *Proceedings of the National Academy of*
094 *Sciences of the United States of America* **98**, (2001).
095 85. Aa, S. *et al.* Regulation of selenoprotein GPx4 expression and activity in human endothelial cells
096 by fatty acids, cytokines and antioxidants. *Atherosclerosis* **171**, (2003).
097 86. Zhang, H. *et al.* Nrf2-regulated phase II enzymes are induced by chronic ambient nanoparticle
098 exposure in young mice with age-related impairments. *Free Radic. Biol. Med.* **52**, 2038–2046
099 (2012).
100 87. Zhou, L., Zhang, H., Davies, K. J. A. & Forman, H. J. Aging-related decline in the induction of
101 Nrf2-regulated antioxidant genes in human bronchial epithelial cells. *Redox Biol* **14**, 35–40 (2018).
102 88. Zhu, Y. *et al.* Increased prefrontal cortical cells positive for macrophage/microglial marker CD163
103 along blood vessels characterizes a neuropathology of neuroinflammatory schizophrenia. *Brain,*
104 *Behavior, and Immunity* **111**, 46–60 (2023).

105 89. Muñoz-Castro, C. *et al.* Cyclic multiplex fluorescent immunohistochemistry and machine learning
106 reveal distinct states of astrocytes and microglia in normal aging and Alzheimer's disease. *J*
107 *Neuroinflammation* **19**, 30 (2022).
108 90. Zeineh, M. M. *et al.* Activated iron-containing microglia in the human hippocampus identified by
109 magnetic resonance imaging in Alzheimer disease. *Neurobiol Aging* **36**, 2483–2500 (2015).
110 91. Reinert, A., Morawski, M., Seeger, J., Arendt, T. & Reinert, T. Iron concentrations in neurons and
111 glial cells with estimates on ferritin concentrations. *BMC Neuroscience* **20**, 25 (2019).
112 92. Li, S. *et al.* RSL3 Drives Ferroptosis through NF-κB Pathway Activation and GPX4 Depletion in
113 Glioblastoma. *Oxid Med Cell Longev* **2021**, 2915019 (2021).
114 93. Belaidi, A. A. *et al.* Apolipoprotein E potently inhibits ferroptosis by blocking ferritinophagy. *Mol*
115 *Psychiatry* 1–10 (2022) doi:10.1038/s41380-022-01568-w.
116 94. Kloske, C. M. & Wilcock, D. M. The Important Interface Between Apolipoprotein E and
117 Neuroinflammation in Alzheimer's Disease. *Front Immunol* **11**, 754 (2020).
118 95. Crapper McLachlan, D. R. *et al.* Intramuscular desferrioxamine in patients with Alzheimer's
119 disease. *Lancet* **337**, 1304–1308 (1991).
120 96. Gleason, A. & Bush, A. I. Iron and Ferroptosis as Therapeutic Targets in Alzheimer's Disease.
121 *Neurotherapeutics* **18**, 252–264 (2021).
122 97. Zhaba, W.-D. *et al.* Deferoxamine reduces amyloid-beta peptides genesis and alleviates neural
123 apoptosis after traumatic brain injury. *Neuroreport* **32**, 472–478 (2021).
124 98. Cacciottolo, M. *et al.* The APOE4 allele shows opposite sex bias in microbleeds and Alzheimer's
125 disease of humans and mice. *Neurobiology of Aging* **37**, 47–57 (2016).
126 99. Reish, N. J. *et al.* Multiple Cerebral Hemorrhages in a Patient Receiving Lecanemab and Treated
127 with t-PA for Stroke. *N Engl J Med* **388**, 478–479 (2023).
128 100. Castellani, R. J. *et al.* Neuropathology of Anti-Amyloid-β Immunotherapy: A Case Report. *J*
129 *Alzheimers Dis* **93**, 803–813 (2023).

130 101. Solopova, E. *et al.* Fatal iatrogenic cerebral β-amyloid-related arteritis in a woman treated with
131 lecanemab for Alzheimer's disease. *Nat Commun* **14**, 8220 (2023).
132 102. Kayed, R. *et al.* Fibril specific, conformation dependent antibodies recognize a generic epitope
133 common to amyloid fibrils and fibrillar oligomers that is absent in prefibrillar oligomers. *Mol*
134 *Neurodegeneration* **2**, 18 (2007).
135 103. Cacciottolo, M. *et al.* OXIDATIVE STRESS FROM TRAFFIC-RELATED AIR POLLUTANTS
136 (TRAP) INDUCES PRO-AMYLOIDOGENIC LIPID RAFT ALTERATION IN AD MODELS.
137 *Alzheimer's & Dementia: The Journal of the Alzheimer's Association* **14**, P1124–P1125 (2018).
138 104. Dimauro, I., Pearson, T., Caporossi, D. & Jackson, M. J. A simple protocol for the subcellular
139 fractionation of skeletal muscle cells and tissue. *BMC Res Notes* **5**, 513 (2012).
140 105. Thorwald, M. A. *et al.* Nrf2-related gene expression is impaired during a glucose challenge in
141 type II diabetic rat hearts. *Free Radic. Biol. Med.* **130**, 306–317 (2019).
142 106. Stolwijk, J. M., Falls-Hubert, K. C., Searby, C. C., Wagner, B. A. & Buettner, G. R.
143 Simultaneous detection of the enzyme activities of GPx1 and GPx4 guide optimization of
144 selenium in cell biological experiments. *Redox Biol* **32**, 101518 (2020).
145